FRACTURE PARAMETERS FOR BURIED CAST IRON PIPES SUBJECTED TO INTERNAL AND EXTERNAL CORROSIONS AND CRACKINGS

by

© Atika Hossain Akhi

A Thesis Submitted to the

School of Graduate Studies

In partial fulfillment of the requirements for the degree of

Master of Engineering

Faculty of Engineering and Applied Science

Memorial University of Newfoundland

May 2021

St. John's Newfoundland and Labrador Canada

Abstract

Cast iron water main represents a significant portion of municipal infrastructure in North America and worldwide. The aging cast-iron pipes are subjected to deterioration due to corrosion, resulting in cracking and failure. The municipalities face problems with pipe breakage or leakage and associated socio-economic issues caused by water loss, service disruption, and damages to the nearby facilities. For a proper maintenance decision of the pipes, it requires evaluating the remaining strength of the deteriorating structure. Fracture mechanics is being preferred to assess the remaining strength of the deteriorating structure over the conventional strength-based method due to its ability to capture crack initiation and propagation. However, determining fracture parameters, such as Stress Intensity Factor (SIF), is a challenge in applying the fracture mechanics for evaluating the structure. This study presents an evaluation of the SIF for buried cast iron pipes subjected to internal and external corrosions and cracks. Semi-elliptical surface defects (crack only and crack with corrosion) are considered for a wide range of aspect ratios (crack-depth to crack-length ratio) and relative crack depths (crack-depth to pipe thickness ratio) to evaluate the SIFs. The SIFs are assessed for invert/crown and springline position cracks under internal pressure and vertical surface loads. The study revealed that the SIF for a crack due to internal pressure is not affected by the presence of surrounding soil and therefore can be calculated using the available solution for in-air pipes. The SIF due to surface load depends on its geometry and location of the crack. A design equation is proposed to calculate the SIFs due to the surface load using an influence coefficient. The influence coefficient is presented for internal and external semi-elliptical defects as a function of crack aspect ratios, depths and locations. A method is proposed to determine the SIFs for buried pipes as a sum of the SIFs due to the internal pressure and the surface loads.

Acknowledgments

First and foremost, I would like to express deep praise and gratitude to the Almighty for giving me strength and patience for this academic journey. I would like to express my sincere gratitude to my graduate supervisor, Dr. Ashutosh Sutra Dhar, for providing invaluable guidance and insight into the studies. Again, I would like to thank Dr. Dhar for his excellent attitude and rich academic background, which would be an unforgettable and lifelong memory for my life.

Special thanks to Suborno Debnath, Pipeline Integrity Specialist at Northern Crescent Inc., for his co-operation at the beginning of this research conduction. I would like to thank other members currently working under Dr. Dhar for being co-operative in different difficulties and their continuous encouragement and knowledge sharing mentality. Finally, I would like to convey my thanks, love and gratitude to my husband, parents and other family members due to their encouragement and sacrifice for my personal and academic life.

Table of Contents

List of Figures

List of Tables

Co-authorship Statement

As the principal author, Atika Hossain Akhi has conducted all the research of the manuscripts presented in this thesis under the direct supervision of Dr. Ashutosh Sutra Dhar. Mrs. Akhi also prepared the draft manuscript. The co-author supervised the research and reviewed the manuscript.

Chapter 1 Introduction and Overview

Buried pipelines are essential underground infrastructure used to transport oil, gas, and water to many communities and industries. Municipal water distribution systems include a large volume of buried pipelines to transport potable water. Cast iron (CI), asbestos cement (AC), concrete steel cylinder (CSC), ductile iron (DI), high-density polyethylene (HDPE), polyvinyl chloride (PVC), molecularly oriented PVC (PVCO), steel are generally used as water mains in USA and Canada and the highest percentage of material (about 28%) used for water mains is cast iron and ductile iron (Baird & Folkman, 2019).

Almost all of the cast iron water mains were installed in the middle of the last century (Folkman, 2018). Based on an investigation, Folkman (2018) reported that 82% of the in-service cast iron pipelines in the USA and Canada already exceeded their design life, and the failure rate of the cast iron water main is considerably higher than the other pipes. The percent distribution of pipes' length based on materials and their breaking rate is illustrated in Figure 1.1. The increase in the break rate of cast iron water main in the USA and Canada during 2012-2018 was 43%. The water infrastructure report card of ASCE categorized the water infrastructure systems in the USA as D grade, indicating that the system is performing below the standard (ASCE, 2017). Canadian Infrastructure Report Card (CIRC) also observed that about 25% of the water main infrastructures are in very poor or fair condition (CIRC, 2019).

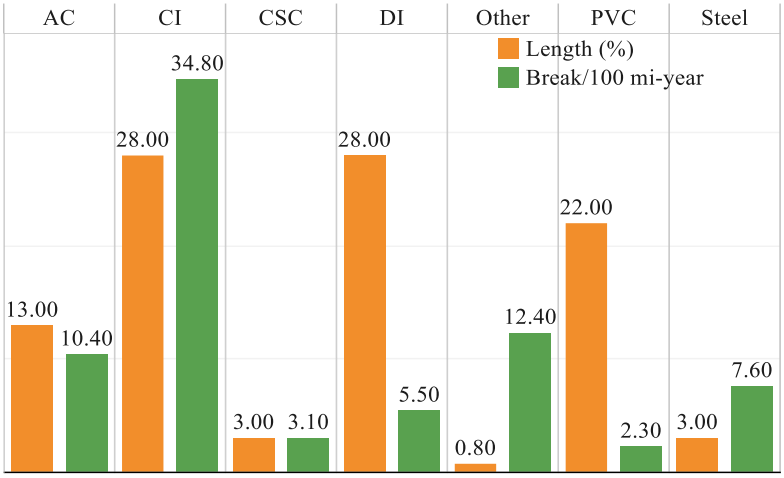

Figure 1.1 Percentage of pipe length and break rate (Folkman, 2018)

The breakage and leakage of the aged pipelines interfere with the continuous supply of water, induce flood damage, and even cause safety issues (Hou et al., 2016). ASCE (2017) published that pipeline breaks cause the wastage of treated drinking water over two trillion gallons annually. American Water Works Association report found the necessity of 1 trillion dollars for fulfilling the water demand in the future. The organization also reported that the delayed investment for the replacement of the deteriorated pipelines might be the cause of the significant increment of water service disruption and the cost of emergency repairs (AWWA, 2017). Therefore, this is crucial to find the causes of pipe failure and the replacement strategy based on the remaining strength.

1.1 Rational of the Current Study

The failures of cast iron water main due to aging has been a concern for the municipalities. Folkman (2018) conducted a detailed survey on the cast iron water mains in the USA and Canada and found the different modes of failures, as shown in Figure 1.2.

The circumferential crack was noticed to be maximum in the cast iron water main. Vipulanandan et al. (2011) found an equal percentage, 37%, of the circumferential and longitudinal cracks for small diameter pipes from the USA's extensive field study. Water pipelines' failures are associated with the pipe and material properties, internal and external loads, and environmental conditions or corrosion.

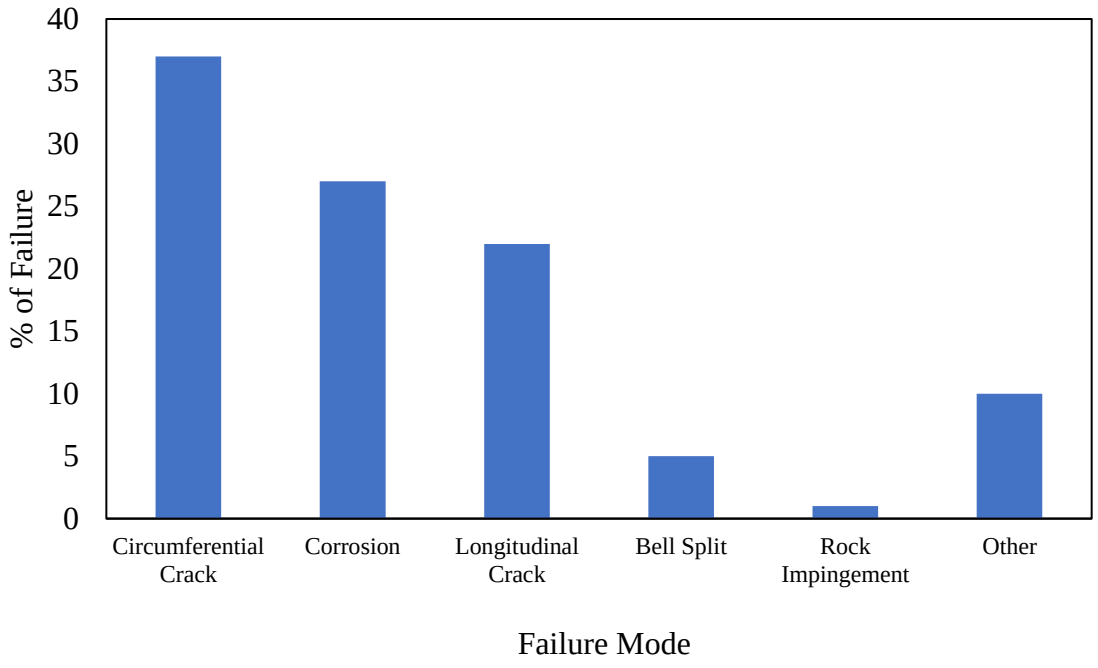

Figure 1.2 Failure Modes in Cast Iron Water Main (Folkman, 2018)

Corrosion in the buried cast iron pipe is the key influencing factor for the initialization of pipe failure. Corrosion can develop on the external and internal surfaces of the pipes. Corrosive soils surrounding the pipeline and water chemistry and flow characteristics are responsible for external and internal surface corrosions, respectively (Rajani & Kleiner, 2013). The corrosion growth leads to the thinning of the pipe wall and reduces the pipe's strength. Material change might also occur due to corrosion, such as

losing toughness. The thinned wall forms localized pitting corrosion with various depths and uneven shapes on the cast iron pipe's internal and external surface. The crack development can initiate from the corrosion pit.

The continuum mechanics is conventionally used for the structural strength assessment of pipelines. In this method, the pipe wall stress is compared with the strength of the material to assess the failure. This approach is not suitable for assessing crack initiation and crack propagation during failure (Debnath & Dhar, 2019) due to its inability to evaluate stress/strain at the locations with singularities (crack tips). Fracture mechanics can overcome the limitations of the conventional method as the stress at the point of singularity is not used in the failure assessment. Researchers are applying fracture mechanics for crack growth and propagation in cast iron water mains for evaluating the remaining life (Wang et al., 2017; Mondal & Dhar, 2019). The application of fracture mechanics facilitates the establishment of pipe failure criteria based on the materials' fracture toughness. Researchers evaluated fracture parameters of crack only defects for in-air cast iron water mains under internal pressure (Raju & Newman, 1982; Fahimi et al., 2016; Wang et al., 2017; Debnath & Dhar, 2019). The buried pipes with crack only defect and crack with corrosion defect were not extensively investigated.

1.2 Objectives and Scope

The major objective of this study is to develop numerical techniques to apply the fracture mechanics for predicting stress intensity factors (SIFs) for the buried cast iron water mains. The specific goals of the thesis are presented as follows:

- To develop a finite element modeling technique to assess the SIF for buried pipes.
- To develop the numerical technique to include the corrosion with crack and obtain the effects of corrosion inclusion on the SIFs.
- To develop the simplified method for calculating the SIFs of buried cast iron pipes.
- To quantify the effect of surface load on the SIFs of internal and external surface cracks of the cast iron buried pipe.
- To assess the effect of the relative crack depth and aspect ratio on the influence coefficients of surface load for both cracks.

Three-dimensional finite element modeling (FEM) technique was employed to determine the fracture parameter for cast iron pipes subjected to internal and external corrosions and cracks. The SIFs under the loading of internal pressure and vertical surface load were investigated to develop a tabular and graphical database for design engineers.

1.3 Thesis Framework

This thesis is written in manuscript format. The outcome of this thesis is presented in five chapters. It includes two manuscripts submitted to the journals (one in Journal of Pipeline Science and Engineering and the other in Engineering Fracture Mechanics). The manuscripts are presented in Chapter 3 and Chapter 4, respectively.

Chapter 1 includes the background of the topic, identification of the research needs, and the objectives and scope of the study.

Chapter 2 provides a brief review of the different aspects of cast iron water pipes, failure modes, and the mechanism of failure and corrosion. The research specific extensive literature reviews are presented in Chapter 3 and Chapter 4.

Chapter 3 includes the manuscript submitted to the Journal of Pipeline Science and Engineering. Fracture parameters for internal surface crack for crack only and crack with corrosion defects are investigated in this chapter.

Chapter 4 presents the manuscript submitted to the Engineering Fracture Mechanics journal. This study evaluates the fracture parameters for external surface crack only and crack with corrosion defects of the buried cast iron water main.

Chapter 5 summarizes the general conclusions, recommendations, and suggestions for future works.

As the thesis is presented in manuscript format, the references for Chapter 3 and Chapter 4 are provided at the end of each chapter. The references cited in Chapters 1, 2, and 5 are listed in the 'Reference' section at the end of the thesis.

Chapter 2 Literature Review

2.1 Introduction

This chapter provides a brief overview of cast iron's mechanical properties, the cast iron pipeline's failure mechanism, and some previous research relevant to the present study. Literature reviews specific to the topics are presented in Chapters 3 and 4. In this thesis, unless stated otherwise, pipelines refer to water main pipelines.

2.2 Historical Background

Cast iron pipe has been an inseparable part of the municipal water supply system since the sixteenth century. Cast Iron Soil Pipe Institute (CISPI) provides a historical overview of the use of cast-iron pipes. According to the document, Germany used cast iron pipe first time in 1562 to supply water to a fountain. The full-scale application of cast iron pipe was recorded in 1664 to distribute water to a 15 miles distance in France. Chelsea Water Company introduced the use of cast iron water pipe in 1746 in London, England (CISPI, 2006).

The earlier use of cast iron pipe was found in North America at the beginning of the nineteenth century. The City of Toronto, Canada first used cast iron pipes in the transmission system in 1870 (Siu, 2018). The extensive use of cast iron pipe in the USA and Canada for water distribution networks was continuous until the middle of the nineteenth century. Based on the manufacturing process, cast iron pipes are categorized as pit cast gray iron and centrifugal cast gray iron pipes. The pit cast gray iron process manufactured the cast iron by pouring molten iron into a sand mold. The centrifugal system

of iron manufacturing was used in 1920 and developed in 1930, which is still in use (Paradkar, 2012).

2.3 Constituents and Properties of the Cast Iron Pipe

Cast iron is chemically composed of iron with some carbon and silicon. The presence of carbon and silicon in cast iron increases fluidity and reduces the melting temperature compared to steel. The typical composition of grey cast iron pipe is as follow: Carbon: 2.5 – 4.0% , Silicon: 1.0 – 3.0%, Phosphorous: 0.002 – 1.0%, Sulfur: 0.02 – 0.25% and Manganese: 0.2 – 1.0% (Martin, 2006). Carbon is present in graphite form in grey cast iron pipe. The presence of graphite flake (Figure 2.1) has a significant influence on the fracture toughness of cast iron pipe (Collini et al., 2008). These flakes act as a void and form natural cracks, producing a brittle fracture (Debnath et al., 2021).

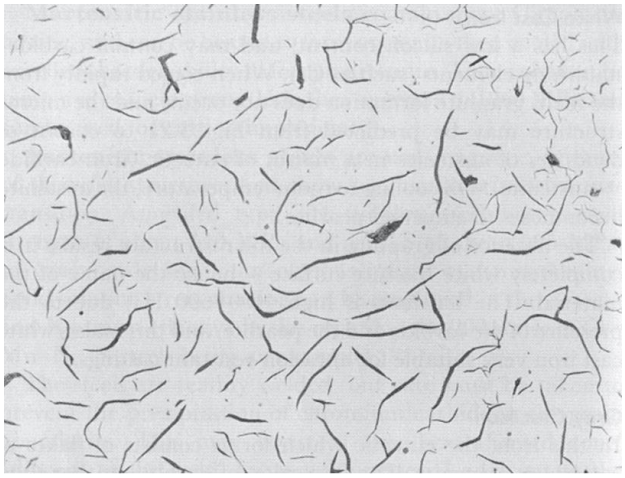

Figure 2.1 Graphite flakes in gray cast iron pipe (Martin, 2006)

The failure mechanism of the aged pipes is related to their mechanical properties such as, tensile strength, compressive strength, rupture modulus and fracture toughness. Seica and Packer (2004) summarized the mechanical properties of the aging pipe reported

by various researchers. The material properties of different cast iron pipes are presented in Table 2.1. The presented information shows a wide variation of the tensile strength, modulus of rupture, fracture toughness of the aged cast iron pipe materials.

Table 2.1 Mechanical properties of cast iron (Seica & Packer, 2004)

Type of cast iron	Reference	Age (years)	Tensile strength (MPa)	Modulus of rupture (MPa)	Fracture toughness (MPa√m)
Pit	Rajani et. al. (2000)	64-115	33-267	132-378	5.7-13.7
Pit and Spun	Conlin and Baker (1991)	Out of service pipes	137-212	n/a	10.5-15.6
Pit and Spun	Seica et. al. (2004)	50-124	47-297	164-349	n/a
Spun	Yamamoto et. al. (1983)	22-79	100-150	20-250	n/a
Spun	Caproco Corrosion (1985)	22-28	70-217	n/a	n/a
Spun	Ma and Yamada (1994)	21-32	40-320	120-320	n/a
Spun	Rajani et. al. (2000)	22-61	135-305	194-445	10.3-15.4

2.4 Failure of Buried Pipe

Breakage and leakage are frequent forms of failure of deteriorating buried cast iron pipes. Breakage occurs when a pipe cannot withstand the internal pressure and external forces acting on it. The deterioration of the pipe with time can reduce the capacity to withstand the forces, which can lead to failure. The factor of safety (the ratio of the structural capacity and stress due to applied forces) of the buried cast iron water main reduces with time due to deterioration, as shown in Figure 2.2. It reaches the breakage stage at the critical value of 1 (Rajani & Kleiner, 2004).

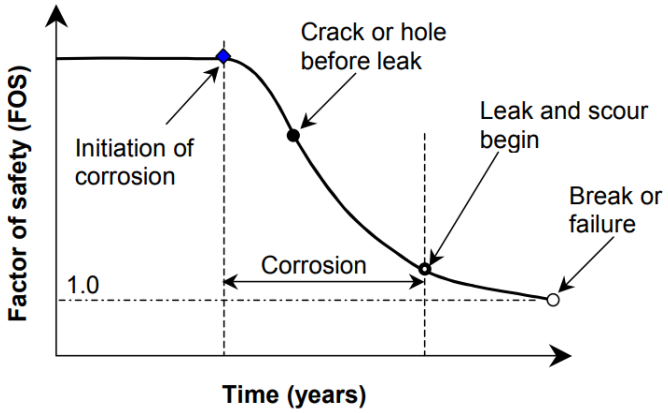

Figure 2.2 Factor of safety of cast iron pipe (Rajani & Kleiner, 2004)

2.5 Corrosion

The corrosion on the interior and exterior surfaces is the major cause of failure for buried cast iron pipes. The electrochemical process prompts the development of corrosion in the metal pipe. Seica et al. (2002) conducted a study on 100 pipe samples from the City of Toronto and found that 95% of the pipes were damaged by medium to severe corrosion. The internal and external surface of the cast iron water main suffered from corrosion. Both surface corrosions pose a threat to the mechanical failure of the pipeline. Besides, internal corrosion produces scale layers and creates water quality problems.

2.5.1 Parameters Affecting Corrosion

The dynamic and complex nature of the surrounding soil, environmental factors and material characteristics influence the corrosion in the buried metal pipes. Corrosion rate on the metal pipe is accelerated with higher moisture content in the soil, low soil resistivity, decreased p^H of the soil, soil texture based on moisture retention and temperature by direct or indirect impacts (Alamilla et al., 2009; Petersen & Melchers, 2012;

Usher et al., 2014). Internal corrosion of the water main is significantly affected by flow characteristics and water chemistryand corrosive soils contribute to induce external corrosions (Rajani & Kleiner, 2013).

2.5.2 Category of Corrosion

There are different corrosion categories identified in the internal surface and external surface of the buried pipe. The common types of corrosion are uniform corrosion, pitting corrosion, tuberculation, galvanic corrosion and crevice corrosion (Liyanage, 2016). Rajeev et al. (2014) collected information on the aged pipes in Australia to determine the pipeline's actual deterioration and defects. Based on the condition assessment, the authors classified the corrosion mainly into three categories comprising general, pit, and patch corrosion.

General corrosion, also called uniform corrosion, occurs in most underground metal pipes due to chemical and electrochemical action. General corrosion reduces the thickness all around the metal pipe (Ji et al., 2017), as shown in Figure 2.3. Localized corrosion on the metal surface is the pitting corrosion shown in Figure 2.4, causing holes on the pipe. The pit with a higher length to width ratio and the very small angle at the bottom is identified as the pipe surface cracks. The concept of fracture mechanics can be employed to describe the behavior of these cracks (Fu et al., 2020).

Figure 2.3 General corrosion (Ji et al., 2017)

Figure 2.4 Corrosion pit (Liyanage, 2016)

Corrosion in the metal pipe is also observed in the form of a large patch or a cluster of individual defects. Figure 2.5 illustrates the corrosion patch in the buried water pipe. Generally, maximum pit depth is an essential factor for assessing corrosion damage in the cast iron pipe. The occurrences of corrosion damage in the cast iron pipeline were mostly observed in the case of corrosion patches (Deo et al., 2019). Ji et al. (2015) evaluated the stress concentration factor as the cast iron pipe's failure criteria, considering the patch dimension.

Figure 2.5 Corrosion patch (Ji et al., 2017)

2.6 Pipe Failure Assessment

Failure of the cast iron water main is characterized based on the loss of strength and the loss of toughness. Cast iron pipe loses its wall thickness due to corrosion on the pipe surface. As a result, stresses on the pipe wall are increased under service loads. If this strength of the material becomes less than the stress associated with internal and external loads, pipeline failure occurs. This condition is stated as a strength limit state. On the other hand, crack defects on the pipe surface prompt the loss of toughness due to stress concentration at the crack tip. When stress intensity on the cracked pipe is higher than the pipe's fracture toughness, pipeline failure occurs. This scenario is described as a toughness limit state (Mahmoodian, 2018).

For the strength limit state-based assessment, Rajani et al. (2000) provided Equations 2.1 and 2.2 to evaluate the total circumferential stress and longitudinal stress on the pipe wall, respectively.

$$\sigma_h = \sigma_{IF} + \sigma_{SW} + \sigma_{FP} + \sigma_{TL} \quad (2.1)$$

$$\sigma_a = \sigma_{TD} + \sigma_{IF} + (\sigma_{SW} + \sigma_{FP} + \sigma_{TL})\upsilon \quad (2.2)$$

Where,

σ_h and σ_a are circumferential stress and longitudinal stress, respectively, and υ is Poisson's ratio.

σ_{IF}, σ_{SW}, σ_{FP}, $\sigma_{TL}$and σ_{TD} are stresses due to internal pressure, soil weight, frost pressure, traffic stress, and temperature differences, respectively.

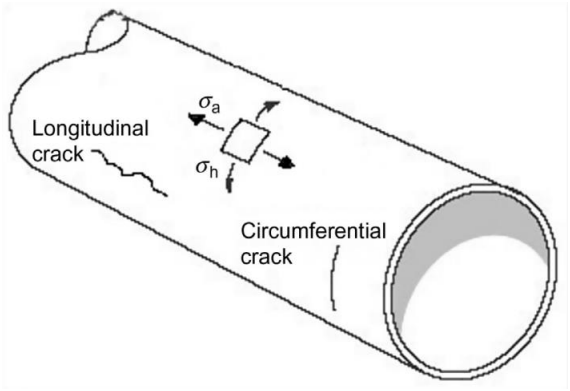

Figure 2.6 Stress and cracks on the pipe wall (Mahmoodian, 2018)

The limit state of circumferential stress and longitudinal stress for the yield strength (σ_y) of the pipe material are presented in Equations 2.3 and 2.4 (Mahmoodian, 2018).

$$G_1(\sigma_y, \sigma_h, t) = \sigma_y - \sigma_h(t) \tag{2.3}$$

$$G_2(\sigma_y, \sigma_{ya}, t) = \sigma_y - \sigma_a(t) \tag{2.4}$$

For the toughness limit state-based assessment, the theory of fracture mechanics is used. Laham (1998) introduced the toughness limit state by introducing relationships for stress intensity near the crack tip. This type of limiting state is applicable for cracks due to pitting corrosion. The stress intensity factor (SIF) for circumferential and longitudinal stress is given in Equations 2.5 and 2.6 (Mahmoodian, 2018).

$$K_{I-c} = \sqrt{\pi a}\sum_{n=0}^{3}(\sigma_n f_n)\left(\frac{a}{d}, \frac{2c}{a}, \frac{R}{d}\right) \tag{2.5}$$

$$K_{I-L} = \sqrt{\pi a}\left(\sum_{n=0}^{3}(\sigma_n f_n)\left(\frac{a}{d},\frac{2c}{a},\frac{R}{d}\right) + \sigma_{bg} f_{bg}\left(\frac{a}{d},\frac{2c}{a},\frac{R}{d}\right)\right) \quad (2.6)$$

Where,

K_{I-c} and K_{I-L} are mode-I SIFs for circumferential and longitudinal stress, respectively.

$a,\ c,\ d,\ and\ R$ are depth of the crack, half-length of the crack, pipe thickness and inner radius of the pipe, respectively.

σ_n and σ_{bg} are the stress normal to the crack plane and the global bending stress, respectively.

f_n and f_{bg} are geometric functions.

The toughness limit state for longitudinal and circumferential cracks for critical SIF, K_C are presented in Equations 2.7 and 2.8, respectively (Mahmoodian, 2018).

$$G_3(K_C, K_{I-L}, t) = K_C - K_{I-C}(t) \quad (2.7)$$

$$G_4(K_C, K_{I-L}, t) = K_C - K_{I-L}(t) \quad (2.8)$$

The SIFs (K_{I-c} and K_{I-L}) depend on the geometry of the defects and the types of loading experienced by the pipe. Researchers are developing simplified methods for design engineers to calculate the SIF under different crack geometries and loading conditions.

2.7 Concept of Linear Elastic Fracture Mechanics

The conventional method applied the strength limit state concept for the failure assessment of structural components. For the failure assessment of corroded or cracked elements, the fracture mechanics concept is used to capture the mechanism of pipe failure (Fahimi et al., 2016; Wang et al., 2017). The application of linear elastic fracture mechanics

(LEFM) is suitable for assessing the fracture parameters. The LEFM is applied in the toughness limit state concept.

Inglis (1913) introduced the basic concept of stress concentration factor for the elliptical hole and observed the influence of geometric features on concentration factors. The major limitation of this concept is that an infinitesimal small stress can lead to the failure of a perfectly elastic plate containing a sharp crack. Griffith (1920) provided an energy balance concept for brittle material, improving the concept. The energy balance concept was also limited to perfectly plastic materials. Irwin (1957) further developed the mechanisms for evaluating the magnitude of stress at crack tip and presented by single parameter named as stress intensity factor near the crack tip. The SIF can be presented by the following Equation 2.9.

$$K = \lim_{r,\theta \to 0} \sigma\sqrt{2\pi r} \tag{2.9}$$

The simplified form of the equation is shown in Equation 2.10. This equation is used for the J-integral based numerical approach for SIF assessment.

$$K = F\sigma\sqrt{\pi a} \tag{2.10}$$

Where,

$K, \sigma, F \; and \; a$ are SIF, nominal stress at failure, geometric factor, and crack depth, respectively.

2.8 Summary

An overview of cast iron material, failure modes, and failure assessment techniques is presented in this chapter. The major causes of the failure of cast iron water mains are the

defects from the corrosion and crack. The conventional methods used continuum mechanics for assessing the failure of the pipe. Researchers are currently applying fracture mechanics for evaluating the failure of corroded and cracked pipes. As cast iron is a brittle material, LEFM can be used for assessing the cast iron pipes.

Chapter 3 Fracture Parameters for Buried Cast Iron Pipes Subjected to Internal Corrosions

Atika Hossain Akhi, Ashutosh Sutra Dhar

Department of Civil Engineering, Memorial University of Newfoundland, St. John's, Newfoundland, CANADA

Abstract

The cast-iron pipeline has been utilized as the water main since the last century and continuously contributes to the present community by supplying potable water. These pipes are subjected to corrosions on the internal and external surfaces, causing pipeline breakage or leakage. For economical maintenance decisions of water distribution networks, it requires assessing the remaining strength of the pipes. Fracture mechanics has been effectively applied for evaluating the remaining strength of deteriorating structures. However, the major challenges in applying the fracture mechanics are obtaining the parameters such as the stress intensity factor (SIF) and fracture toughness. This paper presents a method for calculating the SIFs for cast-iron pipe subjected to internal corrosion. Finite element analysis is employed to calculate the SIFs using the contour-integral method for buried cast iron pipes considering crack only and crack with corrosion defects under internal pressure and vertical surface loads. Various aspect ratios (crack-depth to crack-length ratio) of semi-elliptical defects at the springline and invert/crown of the pipe are considered. The variations of SIFs with the aspect ratio and relative crack depths are represented.

3.1 Introduction

The cast-iron pipeline constitutes a significant portion of municipal water distribution systems. Most of the in-service cast iron water pipes in USA and Canada were installed in the middle of the 20th century (USEPA, 2002). An overwhelming majority (82%) of the pipes exceeded 50 years of their service life and are subjected to deterioration and breaking (Folkman, 2018). Corrosion is regarded as the fundamental cause of pipeline deterioration (Wasim et al., 2020). Corrosive soils (soils containing chemical constituents that can react with metal pipe materials) usually contribute to the corrosion on the external surface (Rajani & Kleiner, 2013; Wasim et al., 2020), and the water chemistry and flow characteristics cause internal corrosion (Rajani & Kleiner, 2013). The consequence of corrosion is the metal loss from the surface, leading to the thinning of the pipe wall. The thinned wall forms localized corrosion pits with various depths and uneven shapes on the internal and external surfaces. The crack development initiates from the corrosion pit (Turnbull, 2014), and subsequently, the crack propagates to pipeline failure (Debnath et al., 2021). The concentration of stress around the crack tip, also known as stress singularity, is considered one of the major causes of pipe failure.

The conventional method of pipeline failure assessment compares the wall stress with the strength of pipe material (Liyanage & Dhar, 2017, 2018; Debnath et al., 2021). The major limitation of this method is its incapability of accounting for crack growth and propagation. To overcome the limitation, researchers employed fracture mechanics for evaluating the remaining strength of pipelines (Fahimi et al., 2016; Wang et al., 2017; Mondal & Dhar, 2019). In fracture mechanics, the strength of the material against cracking

is evaluated using Stress Intensity Factor (SIF), Strain Energy Release Rate (G), J-integral (J), and crack tip opening displacement (δ) (Zhu & Joyce, 2012; Debnath et al., 2021). Stress intensity factor and J-integral term are used for brittle and ductile materials, respectively (Mondal & Dhar, 2019).

Numerous studies were conducted in the past on the pipeline fracture assessment with the internal and external surface cracks of semi-elliptical shapes (Pachoud et al., 2017; Montassir et al., 2020). Raju and Newman (1982) introduced the widely accepted empirical Equation for quantifying SIFs for internal and external semi-elliptical surface cracks of pipes under internal pressures. They considered a wide range of crack depth (a) to crack length ($2c$) ratios with different crack depth (a) to wall thickness (t) ratios. Wang and Lambert (1996) observed the effect of low aspect ratios (a/c = 0.05 and 0.1) with the same relative depths (a/t = 0.2, 0.5, 0.8) on the SIFs for internal and external surface cracks. Li and Yang (2012) performed a finite element (FE) analysis for SIFs of internal surface crack with the high aspect ratio (a/c>1). These studies considered in-air pipes with crack only defects under the internal pressure. The effects of surface load for buried pipes and cracks with metal loss due to corrosion were not considered. Ayatollahi and Khoramishad (2010) used the FE analysis to evaluate the effect of soil pressure on the SIF of a semi-elliptical crack on the internal surface of buried pipelines. They applied soil loads obtained from the closed-form solution of Burns and Richard (1964) on a cylindrical pipe to account for the soil-pipe interaction. However, the solution of Burns and Richard (1964) is only applicable for pipe without any defects, which may not be applicable for a pipe with corrosion defects.

This study aims to address the existing research gaps for the evaluation of SIFs for internal surface corrosions and cracks in cast iron water mains using three-dimensional (3D) FE analysis. The FE models of buried pipes were prepared with semi-elliptical crack-only and crack-with- corrosion defects on the interior surface of different *a/c* and three *a/t*. The analysis was performed using the contour integral method to calculate SIFs along the cracks at the invert/crown and springline positions of the pipe under the loading of internal pressure and surface loads.

3.2 FE Modelling for Internal Defect

FE models were developed to investigate the SIFs for crack only defects and crack with corrosion defects, shown in Figure 3.1 and Figure 3.2, respectively. A commercially available FE software, Abaqus (version 6.14, Dassault Systemes, 2014), was used for the analysis. The standard module of the software (Abaqus/Standard) employs static implicit and dynamic implicit solution algorithms and incorporates the contour integral method, which was used. The FE model was first validated using the available solutions for in-air pipes under internal pressures (i.e., Raju and Newman 1982). The models were then extended for analysis of buried pipes.

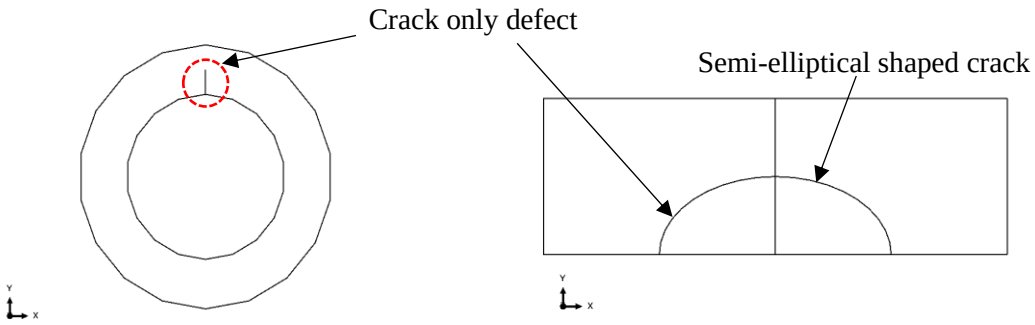

a) Cross-section b) Longitudinal section

Figure 3.1 Internal crack-only defect

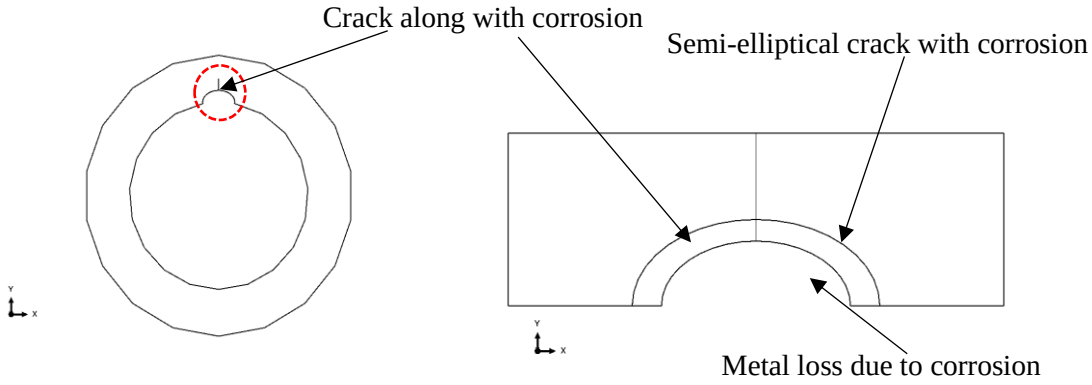

a) Cross-section b) Longitudinal section

Figure 3.2 Internal crack with corrosion defect

Raju and Newman (1982) performed extensive finite element studies for calucating SIFs of semi-elliptical internal surface cracks of in-air pipes and developed the well-known empirical relationship (Equation 3.1).

$$K_1 = \frac{PR}{t}\sqrt{\pi\frac{a}{Q}}F_i\left(\frac{a}{c},\frac{a}{t},\frac{t}{R},\varphi\right) \tag{3.1}$$

Where

$K_1 =$ Mode 1 SIF

$P =$ Radial internal pressure in the cylinder

$R =$ Inner radius of the cylinder

$t =$ Pipe wall thickness

$\frac{PR}{t} =$ Average hoop stress of an uncracked pipe subjected to internal pressure

$a =$ Depth of the surface crack

$Q =$ Shape factor for elliptical crack

$F_i =$ Boundary-correction factor for internal surface crack

$c =$ Half-length of the surface crack

$\varphi =$ Parametric angle of elliptical crack (Figure 3.3)

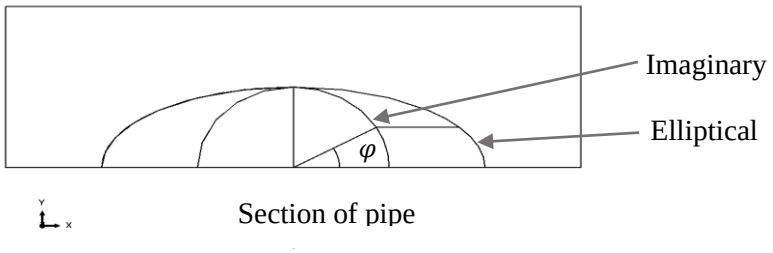

Figure 3.3 Parametric angle (φ) of semi-elliptical internal crack

The shape factor, *Q*, can be obtained from Equation 3.2, Raju and Newman (1982):

$$Q = 1 + 1.464\left(\frac{a}{c}\right)^{1.65} \quad \text{For a} \leq \text{c} \tag{3.2}$$

The boundary-correction factor, F_i is expressed as in Equation 3.3 using influence coefficients for j^{th} (j=0,1,2,3) stress distribution on the crack surface (Raju and Newman, 1982):

$$F_e = \frac{t}{R}\left(\frac{R_0^2}{R_0^2 - R^2}\right)\left[2G_0 - 2\left(\frac{a}{R}\right)G_1 + 3\left(\frac{a}{R}\right)^2 G_2 - 4\left(\frac{a}{R}\right)^3 G_3\right] \quad (3.3)$$

Where,

$R_0 =$ Outer radius of the cylinder

$G_0, G_1, G_2,\ G_3 =$ Influence factors for four polynomial terms for uniform, linear, quadratic, and cubic distributions

The above solution of Raju and Newman (1982) was used for validation of FE models for the in-air pipe. The FE models were prepared for different *a/c* and *a/t* used in Raju and Newman (1982). The calculated SIFs from FE analysis were then compared with those from Equation (3.1). The *a/c* and *a/t* values were maintained by changing *a* and *c* values.

3.2.1 FE Model for In-Air Pipe

Table 3.1 presents the simulation parameters employed for the in-air pipe. The cast-iron pipe was considered as linear elastic materials and characterized by a Young's modulus and a Poisson's ratio. The material parameters were selected based on test results presented in Debnath and Dhar (2019). A pipe of 220 mm outer diameter with a wall thickness of 10 mm was investigated under an internal pressure of 600 kPa for different *a/c* and *a/t*.

Table 3.1 Simulation parameters for pipe materials and internal cracks

Parameters	**Value**
Young's Modulus, E (GPa)	125
Poisson's Ratio, ν	0.25
Density (gm/cm^3)	7.88
Internal Pressure (kPa)	600
Outer Diameter, D_0 (mm)	220
Inner Diameter, D (mm)	200
Relative Wall Thickness (t/R)	0.1
Aspect Ratios (a/c)	0.2, 0.4, 1.0
Relative Depths (a/t)	0.2, 0.5, 0.8

The geometry of the solid pipe is modeled as a 3D deformable body. The application of the contour integral method for calculating SIF requires defining i) the crack front along crack tips, ii) the contours on a plane perpendicular to the crack front that passes through a crack tip, and iii) crack extension direction perpendicular to the crack front (see Figure 3.4). The crack front is defined along element boundaries through a semi-ellipse with the center located on the inner face of the pipe. To create element boundaries along the semi-ellipse, the pipe wall is partitioned, as shown in Figure 3.5. A semi-elliptical shape was extended through the whole pipe circumference using the sweep technique in Abaqus to make the partition (Figure 3.5). The crack tip can be located at any point (nodal points) along the crack front (semi-elliptic boundary). Contours for evaluating contour integral, which is path-independent, can be defined using element boundaries on a plane

perpendicular to the semi-elliptical crack front. To assist in defining circular contours (element boundaries), the pipe wall was partitioned again with the crack front at the center of a circle extending over the full length of the crack (Figure 3.6). It also facilitates generating fine mesh around the crack front/tips, required for the accuracy in the results (Li & Yang, 2012; Randeniya et al., 2016). During finite element mesh generation, the singularity around the crack front is accounted using quadrilateral or brick elements with a collapsed side to induce wedge-shaped elements (Figure 3.6) (Dassault Systemes, 2014).

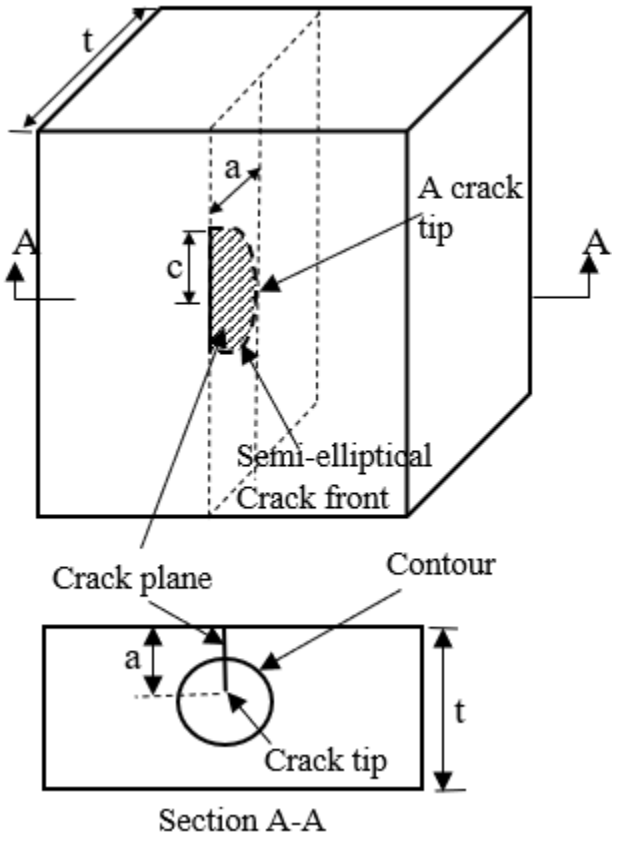

Figure 3.4 Definition of crack parameters

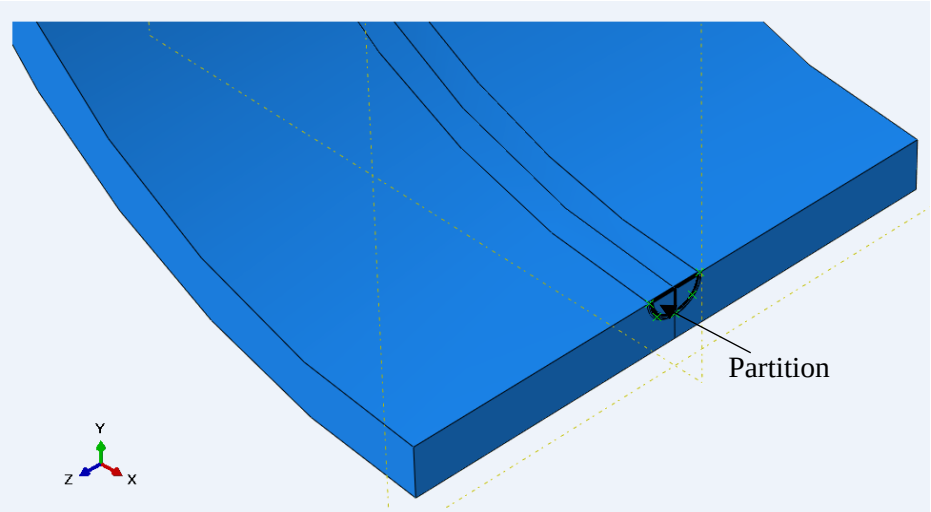

Figure 3.5 Partitioning to define semi-elliptical element boundary for internal crack

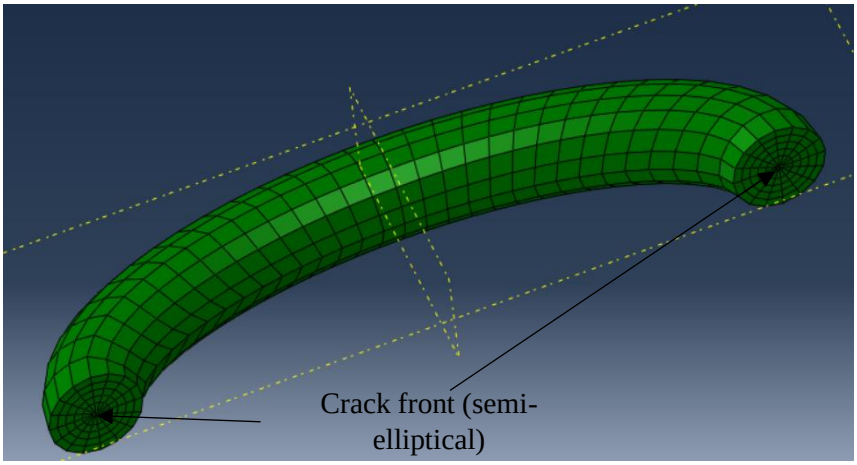

Figure 3.6 Partitioning to define circular element boundaries around the crack front of an internal crack

The virtual crack extension direction is assigned on the crack plane orthogonal to the crack front (perpendicular to the ellipse), varying along the semi-elliptical crack front. For assigning the crack extension direction in Abaqus, a vector (*q* vector) was defined. The input data file is edited to define the *q* vectors at each node, ensuring orthogonality to the

crack front (Figure 3.7). A seam is assigned as overlapping nodes that allow the crack to open in the crack extension direction when loaded.

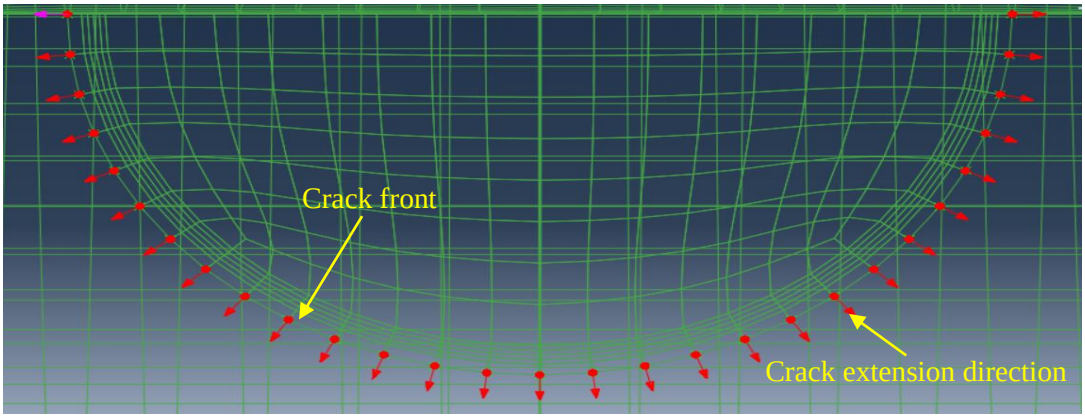

Figure 3.7 Crack extension direction of a semi-elliptical internal crack

Five contours were specified using Abaqus commands to observe SIF values (contour integrals). Abaqus automatically selects each ring of contour line along the element boundaries around the crack front. Figure 3.8 shows the five contours and the crack. The first contour usually provides abrupt results due to the effects of singularity and is ignored (Dassault Systemes, 2014).

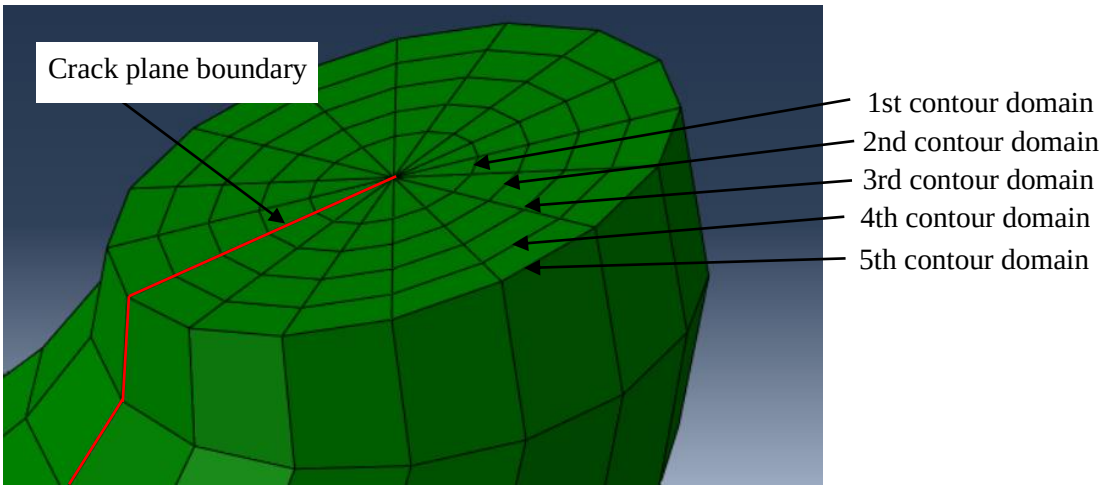

Figure 3.8 Five contours domain around an internal crack line

For the analysis of the in-air pipe, the longitudinal displacements of the pipe were restrained at the end planes by using roller supports while uniform internal pressure was applied. A parametric study was conducted to identify geometric parameters, element types, and mesh size saving computational time. Randeniya et al. (2016) reported that the effects of pipe length on the results are minimized for the ratio of pipe length (L) to half-crack length (c) of greater than 20. Analysis with various pipe lengths was conducted to examine the effect, and $L/c > 20$ was used to minimize the pipe length effects.

Twenty-nodded brick elements with reduced integration (C3D20R) and eight-nodded linear brick elements (C3D8R) with wedge element of C3D15 (15-node quadratic triangular prism element) or C3D6 (6-node linear triangular prism) were first examined to choose the element type. The higher-order elements (i.e., C3D20R and C3D15) may provide more accurate results but may significantly increase the computational time, depending on the types of problems analyzed. For the problem investigated here, no

significant difference in SIF was observed for changing the element types. Thus, C3D6 wedge elements (around crack tips) with C3D8R were used to save computational time. A mesh convergence study was also performed to minimize the mesh size dependency of the results. The same SIFs were calculated along each of the contours (Figure 3.9), confirming the accuracy of the modeling technique.

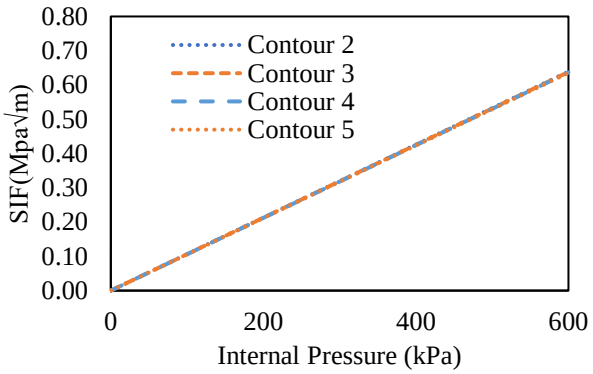

Figure 3.9 SIF for four contours for an internal crack (φ = 0° or φ = 180°)

The SIFs calculated using the FE analysis are compared with those from the semi-empirical equation of Raju and Newman (1982) in Figure 3.10 for various *a/t* and *a/c*. The comparison is presented for in-air pipe with crack only defects. Figure 3.10 shows that the results from FE calculation match well with those from the semi-empirical equation, validating the model. The maximum differences were observed for *a/t* = 0.8, which was less than 5%. Randeniya et al. (2016) and Debnath and Dhar (2019) also reported a difference of less than 5% of FE calculations from those of Raju and Newman (1982) for *a/c* = 1. Note that for lower *a/c* (0.2 and 0.4), the SIF is the maximum at the center of the crack (i.e., φ = 90°). Thus, the crack would propagate from its center to increase the depth.

However, for circular crack (a/c = 1), the SIF is the highest at the edges (φ = 0°, 180°), which may cause an increase of crack-length through propagation from the edges.

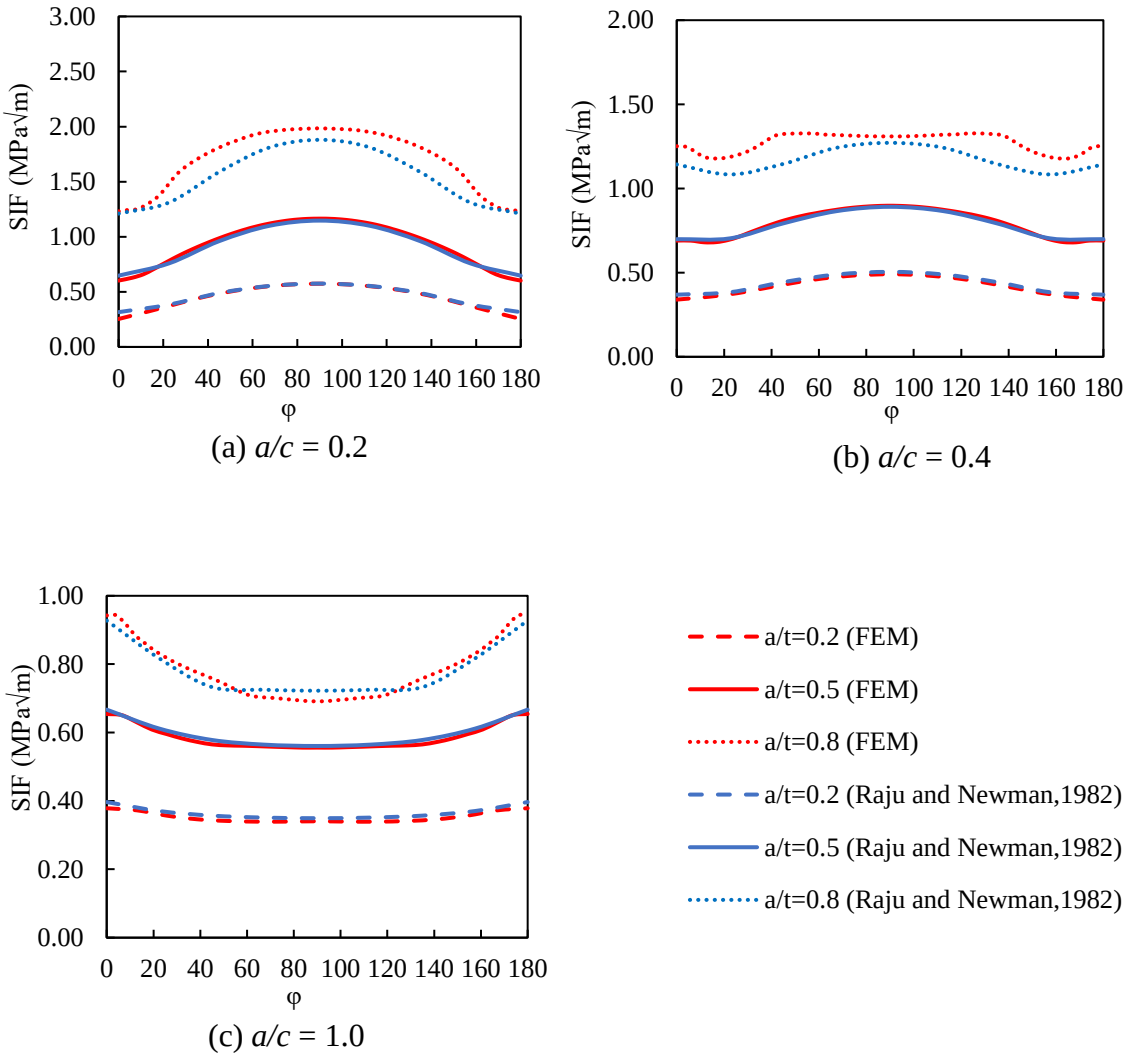

Figure 3.10 Comparison of SIFs from FEM and Raju and Newman (1982)

3.2.2 FE Model for Buried Pipeline with Internal Defect

The finite element models for in-air pipe, discussed above, were used to assess the SIFs for buried pipes with wall cracks using 3D pipe-soil interaction analysis. The soil surrounding the pipe was modeled as elastic-perfectly plastic material defined by the Mohr-Coulomb failure criteria. Typical properties of medium dense sand were assumed for the soil, as shown in Table 3.2. A small value of cohesion was assumed for the sand for the sake of numerical stability. The soil-pipe interface was simulated using the general contact algorithm. The interface friction coefficient was assumed as 0.30.

Table 3.2 Simulation parameters for surrounding soil

Material Properties	**Soil**
Density (gm/cm^3)	1.77
Young's Modulus (MPa)	24
Poisson's Ratio	0.25
Friction Angle in (°)	38
Dilation Angle in (°)	8
Cohesion (kPa)	0.1

The extent of soil in each direction from the pipe is sufficiently far (~10D) to avoid the boundary effects. The length of the model is the same as the length of the in-air pipe, discussed above, with $L/c > 20$. Since the bending is negligible for the pipe buried in the uniform ground, the length is not expected to affect the results. The bottom boundary was restrained from any movement, and the side boundaries were provided with roller support

to restrain any lateral movement. SIFs were calculated for three crack locations, such as crown, springline, and invert of the pipe. The advantages of symmetry were taken for analysis of springline crack. The symmetric boundary condition was applied at the plane of symmetry. Figure 3.11 shows the finite element mesh used.

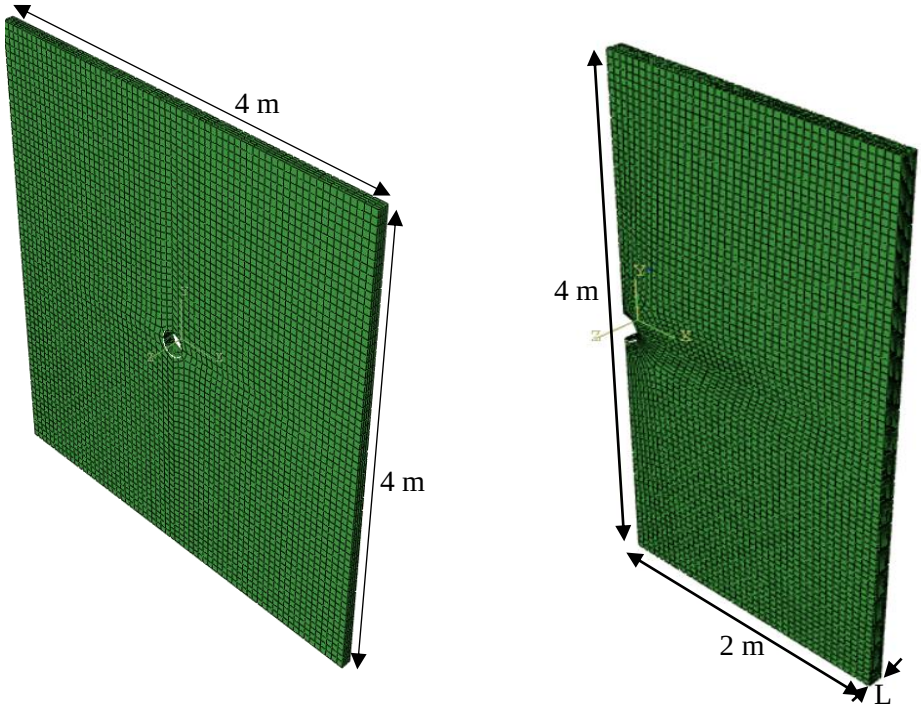

(a) Crown/invert crack analysis (b) Springline crack analysis

Figure 3.11 FE model for soil-pipe interaction analysis for an internal crack

Two load steps were applied during the analysis. In the first step, an internal pressure of 600 kPa was applied. Then, a surface load equivalent to the weight of 2 m of soil (i.e., 34.73 kPa) was applied at the top boundary. The results from the first step were compared with those from the solution of Raju and Newman (1982) to examine the suitability of the semi-analytical equation in calculating the SIF for the buried pipe. The

results from the second step provide the SIFs due to the combined application of surface load and internal pressure.

3.3 Results

3.3.1 Buried Pipes with Crack Only Defects

A study was first conducted to investigate SIFs for a crack oriented in circumferential and longitudinal directions of the pipe that revealed significantly higher SIFs for the longitudinal crack than for the circumferential crack. Similar results were also reported in Debnath and Dhar (2019) for pipes under internal pressure and a uniform surface load. The SIFs for longitudinal cracks are, therefore, presented in the current study.

Figure 3.12 and Figure. 3.13 plot the SIFs for the buried pipes with springline cracks and crown/invert cracks, respectively. The SIFs are calculated under internal pressure without and with surface load for semi-elliptical longitudinally oriented internal cracks with various aspect ratios (a/c = 0.2, 0.4, 1.0) and the relative crack depths (a/t = 0.2, 0.5, & 0.8). The SIFs for invert and crown cracks were equal as plotted in Figure 3.13. Figure 3.12 reveals that the SIFs for springline crack is reduced for application of the surface load. The reduction of SIF is attributed to the compressive bending stress on the interior surface under the surface load. The highest SIFs under the combined load (internal pressure and surface load) are located at the center of the cracks, as in internal pressure loading, for a/c of 0.2 and 0.4. However, for circular crack, the location of the highest SIF moved from the edges for internal pressure loading to the center for the combined load.

For the crown or invert crack, the SIFs increase for application of the surface load (Figure 3.13) due to the tensile bending stress on the pipe's inner surface. The location of the highest SIFs depends on the magnitudes of *a/c* and *a/t*. The maximum SIFs are generally located at the center of the crack for lower *a/c*. For *a/c* = 0.4, the SIF is the maximum at the crack edges for a deeper crack (*a/t* = 0.8). As observed for springline crack, the maximum SIFs are located at the edges for circular cracks (*a/c* = 1.0).

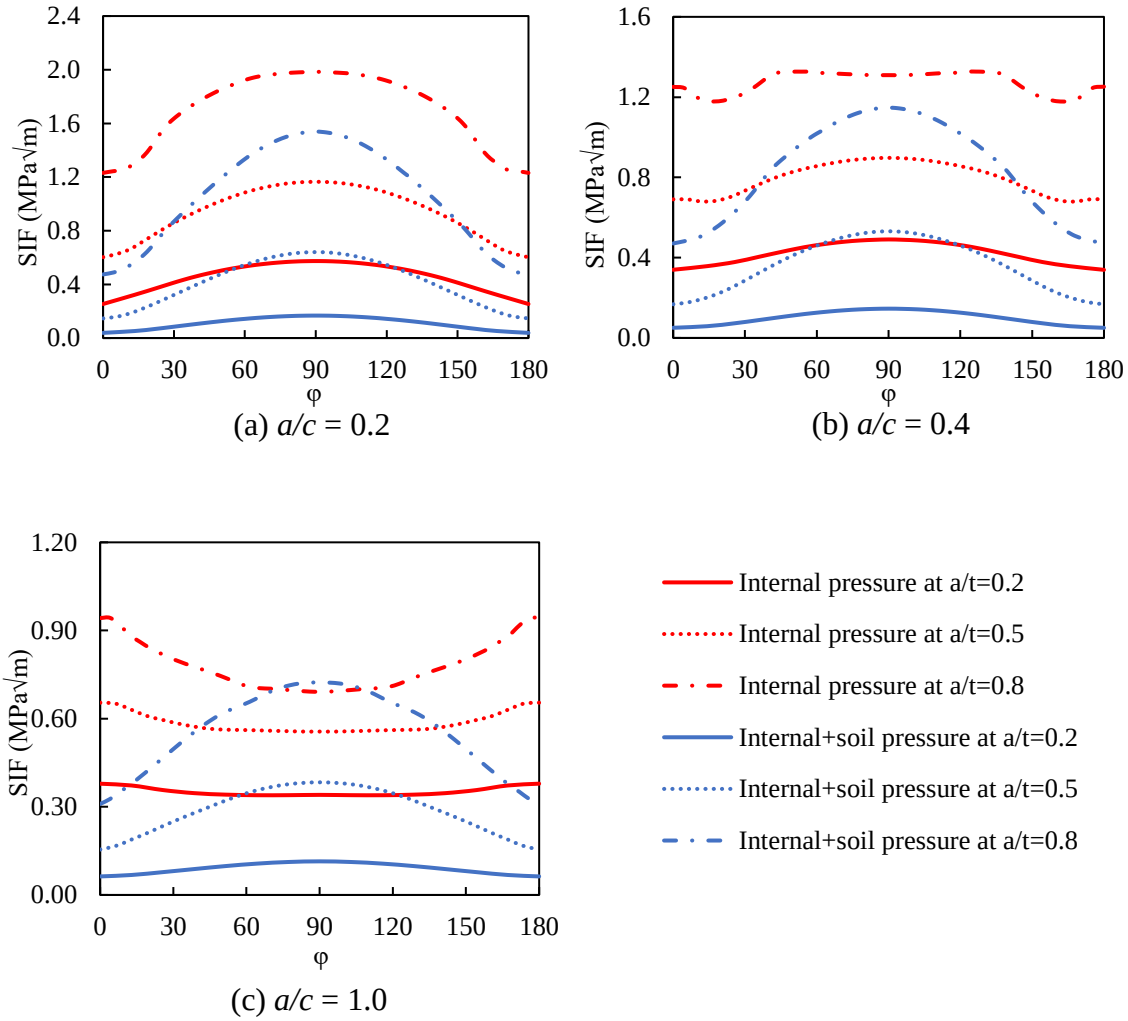

Figure 3.12 SIFs for internal springline crack of a buried pipe

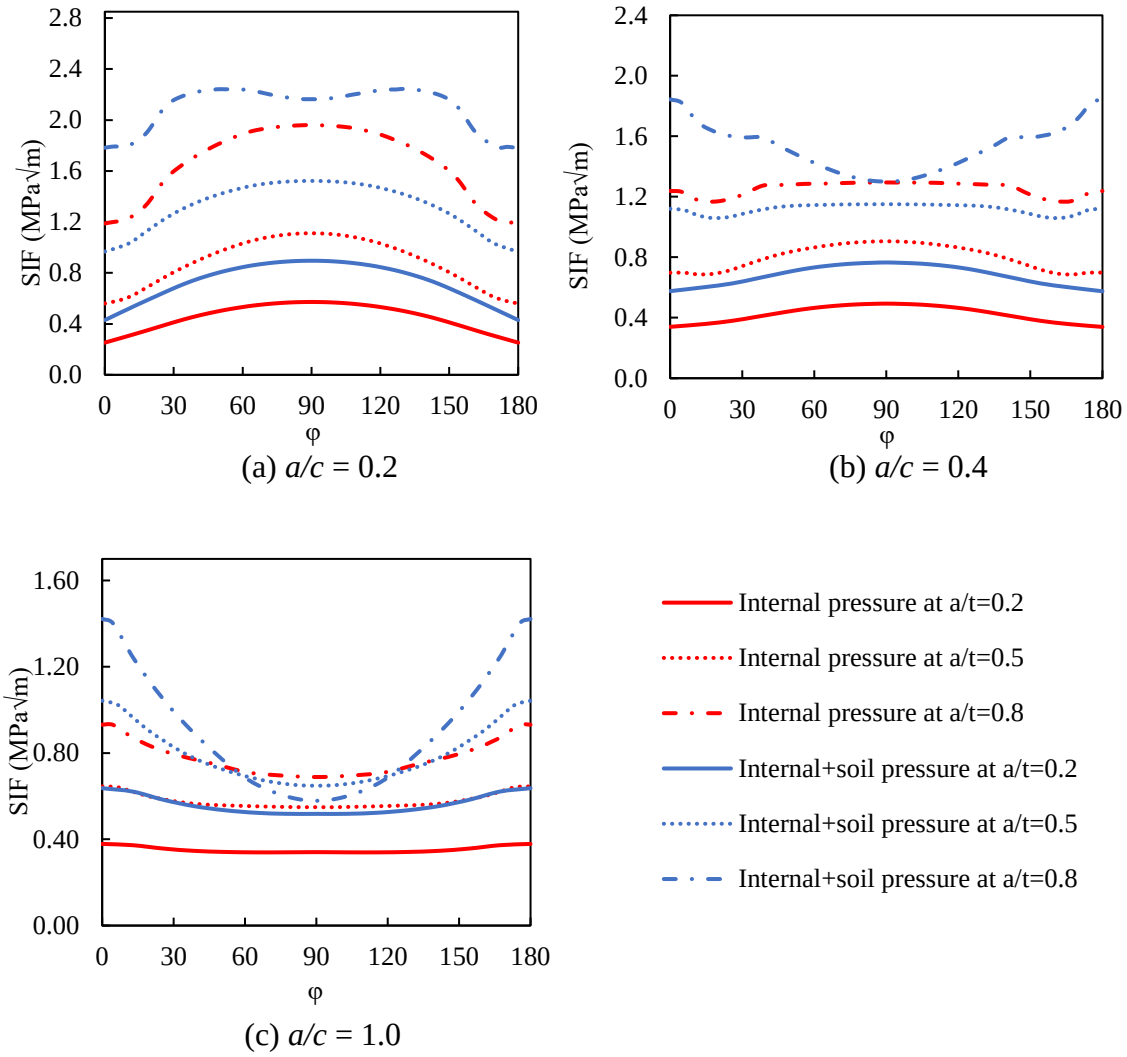

Figure 3.13 SIFs for internal invert/crown crack of a buried pipe

Figure 3.14 compares the SIFs under internal pressure for the buried pipe and those for in-air pipe obtained from the equation of Raju and Newman (1982). The SIFs for the buried and in-air pipes match reasonably shown in the figure. Thus, the equation of Raju and Newman (1982), developed for the in-air pipe, can be used for the buried pipe under internal pressure. The SIFs under the surface load can be separately calculated and added

to the SIFs under the internal pressure to obtain the total SIFs. The SIFs for a buried pipe can be expressed as in Equation 3.4 (Debnath & Dhar, 2019).

$$K_{total} = K_{pressure} + K_{surface} \quad (3.4)$$

Where,

K_{total} = Total SIF

$K_{pressure}$ = SIF due to internal pressure to be calculated using Raju and Newman (1982) equation

$K_{surface}$ = SIF due to surface load

In the current study, the SIF due to surface load ($K_{surface}$) was investigated for different crack dimensions using FE analysis. Based on the study, a simplified method for calculating $K_{surface}$ is provided, as discussed later in the paper.

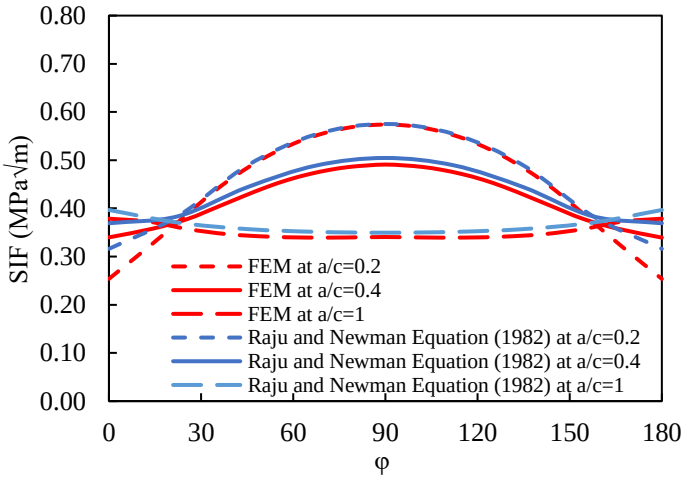

Figure 3.14 SIFs due to internal pressure for in-air and buried pipes with an internal crack

3.3.2 Buried Pipe with Internal Crack-with-Corrosion Defects

SIFs for a 'crack with corrosion defect' on a pipe were calculated considering half-ellipsoidal corrosion (Figure 3.15). Analysis with the Extended Finite Element Method (XFEM) was first performed with the corroded pipe to identify the location of the crack, which was essentially in the longitudinal direction at the center of the corrosion (Figure 3.15b). A semi-elliptical crack is then defined with a total defect depth of 5.00 mm (a corrosion depth of 3.0 mm and a crack depth of 2.0 mm) at the identified location of the crack (Figure 3.15a). The results of the analysis were compared with those with a 5 mm deep crack-only defect.

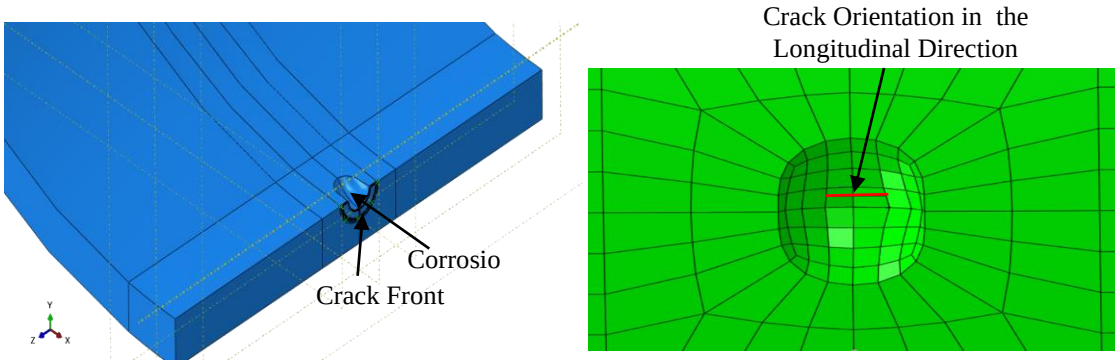

(a) Corrosion and crack (b) Crack location from XFEM analysis

Figure 3.15 An internal crack with a semi-ellipsoidal corrosion defect

Figure 3.16 shows a comparison of SIFs for crack-only defect and crack with corrosion defects for different aspect ratios (a/c) and a relative depth of a/t = 0.5. The results for buried pipe under the combined application of internal pressure and surface load are shown in the figure. In the figure, the SIFs for the crack-only defect and the crack with corrosion defect match with each other for the invert/crown crack and match reasonably

(within 5%) for springline crack. Debnath and Dhar (2019) also reported for *a/c* =1.0 that the SIF values for crack only and crack with corrosion defects with the same total defect depth are almost the same. Thus, the total defect depth can be used to calculate the SIFs for 'crack with corrosion defect' using the solutions developed from crack-only defects. The Raju and Newman' equation can be used to calculate the SIFs for the pipe subjected to internal pressure loading (Raju & Newman, 1982). The contribution of the surface load on the SIFs can then be added to obtain the SIFs for the combined load. A simplified method is developed to calculate the contribution of surface load on the SIF, as discussed below.

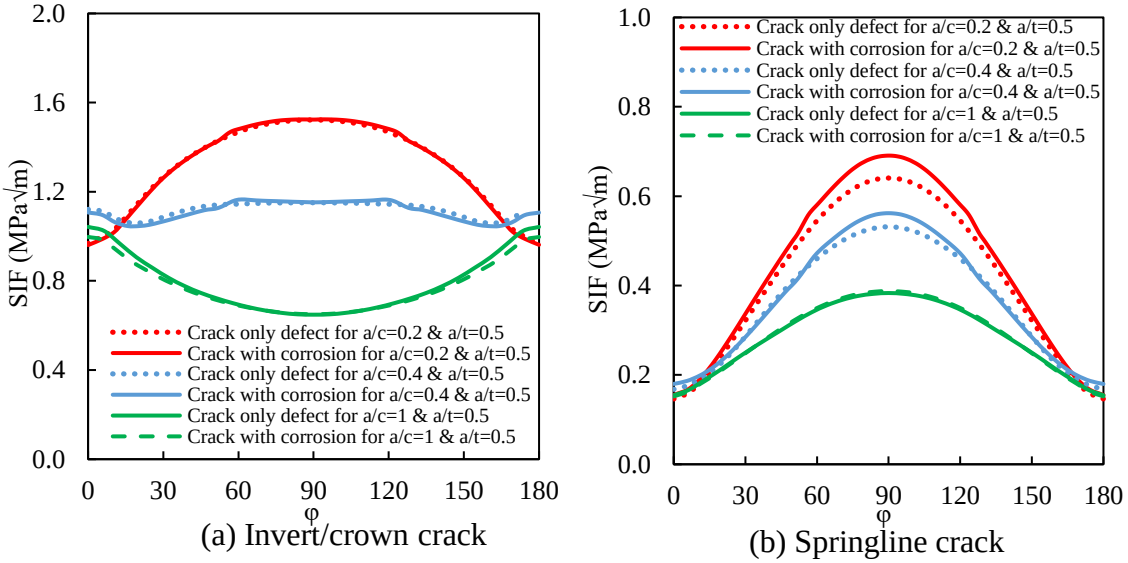

(a) Invert/crown crack (b) Springline crack

Figure 3.16 SIF for internal crack only and crack with corrosion defects

3.3.3 SIFs of Internal Crack for Surface Load

Debnath and Dhar (2019) proposed a simplified equation for calculating SIF for the semi-circular crack on the exterior surface of the buried pipeline due to surface load (Equation 3.5).

$$K_{surface} = q\sqrt{\pi \frac{a}{Q}} F_s\left(\frac{a}{c}, \frac{a}{t}, \frac{t}{R}, \varphi\right) \tag{3.5}$$

Here,

$q =$ surface load. The surface load was applied to simulate the gravity load calculated as $q = \rho g h$ where ρ, g and h are density, acceleration due to gravity, and depth of soil cover, respectively.

F_s = Influence coefficient, which is a function of *a/c*, *a/t*, *t/R* and φ.

Q = Shape parameter defined as below:

$$Q = 1 + 1.464\left(\frac{a}{c}\right)^{1.65} \qquad for\ \frac{a}{c} \leq 1 \tag{3.6}$$

$$Q = 1 + 1.464\left(\frac{c}{a}\right)^{1.65} \qquad for\ \frac{c}{a} \leq 1 \tag{3.7}$$

Assuming that Equation 3.5 is applicable for elliptical cracks, the influence coefficients are back-calculated based on the SIFs obtained from FE analysis. The SIFs due to surface load ($K_{surface}$) were obtained from the FE results using Equation 3.5. The influence coefficients, F_s for different aspect ratios (*a/c* = 0.2, 0.4, 1.0) and relative depths (*a/t* = 0.2, 0.5, 0.8) for different parametric angles are presented in Table 3.3. As seen in the table, the influence coefficient is negative for springline crack and positive for invert

crack, indicating an adverse effect of surface load on the invert/crown crack. The influence factors proposed in Table 3.3 can be used for calculating SIFs for crack only and crack with corrosion defects (using the total depth of defect).

Table 3.3 Influence coefficients for internal surface cracks

a/c	**Crack depth**	**Springline**			**Invert**		
		a/t			***a/t***		
	Angle	**0.2**	**0.5**	**0.8**	**0.2**	**0.5**	**0.8**
0.2	0	-89.90	-120.53	-158.05	73.91	107.67	124.11
	π/8	-126.50	-137.10	-158.49	103.55	119.13	118.78
	π/4	-153.42	-144.25	-144.76	123.85	120.30	96.85
	3π/4	-166.20	-141.15	-111.72	132.85	112.93	61.10
	π/2	-169.82	-138.43	-93.06	135.20	108.53	42.19
0.4	0	-120.80	-138.12	-162.99	98.56	111.68	126.47
	π/8	-126.78	-120.75	-124.09	102.81	94.68	90.53
	π/4	-135.48	-112.66	-91.69	108.38	83.29	54.66
	3π/4	-142.06	-101.43	-51.82	112.61	70.23	17.78
	π/2	-144.14	-96.69	-33.82	113.71	64.82	1.20
1.0	0	-179.95	-180.21	-180.39	147.33	143.18	139.69
	π/8	-162.87	-136.95	-110.55	132.19	104.39	77.36
	π/4	-142.98	-95.63	-47.33	114.28	67.06	19.95
	3π/4	-131.98	-71.15	-5.77	104.06	44.07	-17.65
	π/2	-128.99	-62.28	9.15	101.15	35.85	-31.44

The influence factors for springline and invert/crown cracks for different aspect ratios are graphically presented in Figure 3.17. As shown in Figure 3.17, the influence factor at the center of the crack decreases for the crown/invert crack and increases (negative magnitude reduces) for the springline crack with the increase of *a/t*. The figure shows negative magnitudes of F_s for springline cracks (except for *a/c* =1 and *a/t* = 0.8) and positive magnitudes for the crown or invert cracks (except for *a/c* = 1 and *a/t* = 0.8). As mentioned earlier, the compressive stress on the inner pipe surface at the springline, due to surface load, can lower the stress intensity factor, resulting in a favorable effect. However, the surface load has an adverse effect on the crown or invert cracks, increasing the SIFs. The magnitudes of Fs in Figure 3.17 can be used to calculate the increase in the SIF from Equation (3.5).

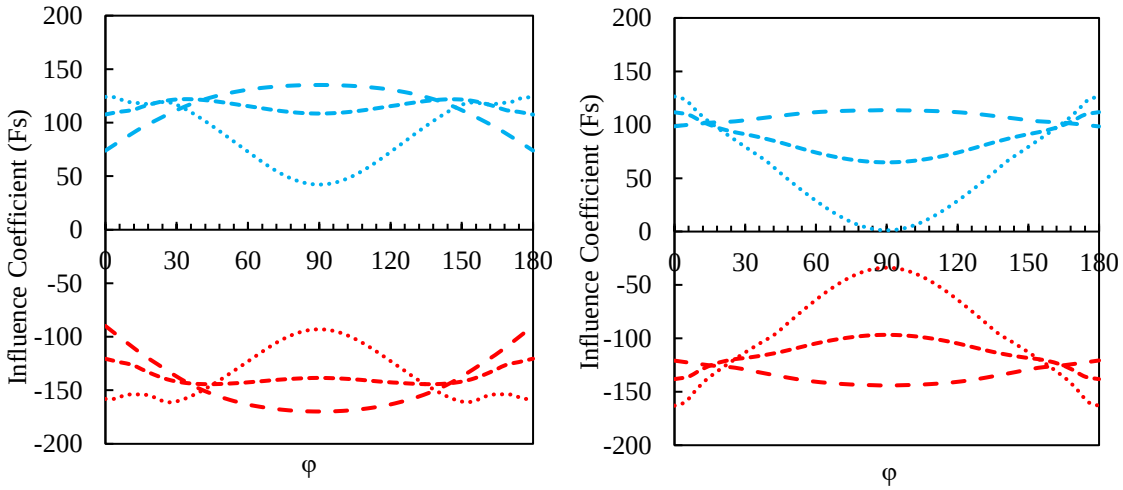

(a) *a/c*=0.2

(b) *a/c*=0.4

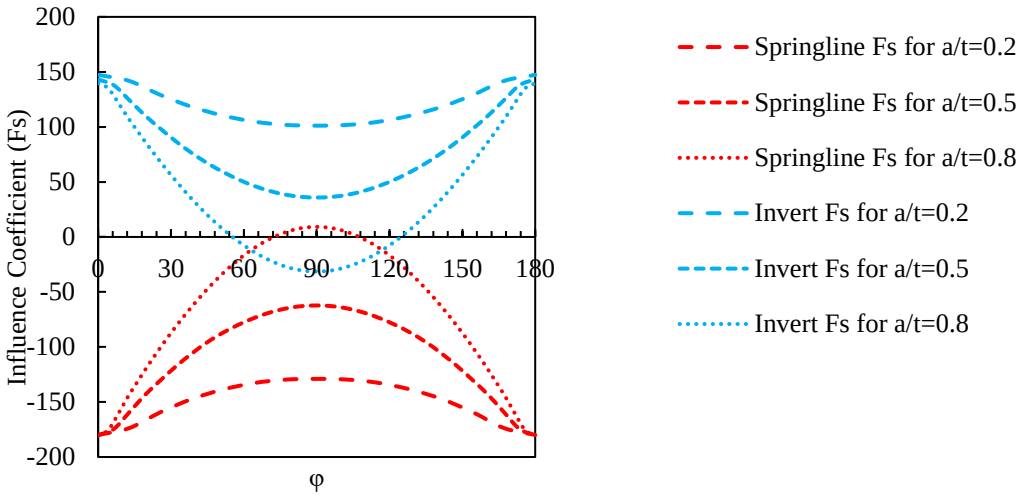

(c) *a/c*=1.0

Figure 3.17 Influence factors for internal cracks due to surface load

3.4 Conclusions

This paper presents an FE investigation of the SIFs for longitudinally oriented semi-elliptical cracks on the internal surface of buried cast iron pipes. The analysis was performed for crack only and crack with corrosion defects under the internal pressure and surface load. The SIFs were examined for different aspect ratios (*a/c*) and relative depths (*a/t*) of the cracks. The major findings from the study are as below:

- The longitudinal crack is the most critical for buried pipes under internal pressure and surface loads.
- The presence of the surrounding soil does not influence the SIFs due to internal pressure. Thus, the equation of Raju and Newman (1982) can be used to calculate the SIFs for buried pipes under internal pressure loading.

- The surface load reduces the SIFs of springline crack due to compressive bending stress in the interior pipe wall and increases the SIFs for invert/crown cracks due to tensile bending stress. The SIFs due to combined load can be obtained by adding the contribution of the surface load to the SIFs due to internal pressure. New influence coefficients are proposed for calculating SIFs under surface load.
- The crack on corrosion defects can be treated as a crack-only defect for SIF calculation using the total depth of defects as the corrosion depth plus the crack depth.
- For an elliptical crack with low aspect ratios (low *a/c*), the SIF is the maximum at the crack's center, indicating the crack depth increase when loaded. For a high aspect ratio or circular crack, the SIF is higher near the crack's edge, indicating the crack length increase.
- Shape parameters, *a/c,* and *a/t* significantly affect the influence factors for the surface load. Changes in the values of the parameters with the parametric angle significantly change the influence factors, hence, the SIF.
- The analysis presented in this study was conducted assuming linear elastic properties of the pipe material, and elastic perfectly-plastic properties of the soil. The applicability of the results is also limited to the pipe and soil parameters considered.

3.5 References

Ayatollahi, M. R., & Khoramishad, H. (2010). Stress intensity factors for an axially oriented internal crack embedded in a buried pipe. *International Journal of Pressure Vessels and Piping, 87*(4), 165–169. https://doi.org/10.1016/j.ijpvp.2010.02.005

Burns, J. Q., & Richard, R. M. (1964, September). Attenuation of stresses for buried cylinders. *Proceedings of Symposium on soil structure interaction. Tucson, Arizona: University of Arizona; 1964*. 378-392.

Dassault Systemes. (2014). *ABAQUS/CAE user's guide*. Dassault Systemes Simulia Corp. Providence, RI, USA.

Debnath, S., Ali, I. M., Dhar, A. S., & Thodi, P. N. (2021). Material properties for fracture mechanics based strength assessment of cast iron water mains. *Canadian Journal of Civil Engineering*, *48(1)*, 62–74. https://doi.org/10.1139/cjce-2019-0229

Debnath, S. & Dhar, A.S. (2019). Assessment of stress intensity factor for buried cast iron pipeline using finite element analysis. *72nd Canadian Geotechnical Conference (GeoSt.John's 2019), September 29 - October 2, 2019, St,John's, NL, Canada*.

Fahimi, A., Evans, T. S., Farrow, J., Jesson, D. A., Mulheron, M. J., & Smith, P. A. (2016). On the residual strength of aging cast iron trunk mains: Physically-based models for asset failure. *Materials Science and Engineering*, *663*, 204–212. https://doi.org/10.-1016/j.msea.2016.03.029

Folkman, S. (2018). Water main break rates in the USA and Canada: A comprehensive study. *Mechanical and Aerospace Engineering Faculty Publications*, March, 1–49. https://digitalcommons.usu.edu/mae_facpub/174

Li, C. Q., & Yang, S. T. (2012). Stress intensity factors for high aspect ratio semi-elliptical internal surface cracks in pipes. *International Journal of Pressure Vessels and Piping, 96–97*, 13–23. https://doi.org/10.1016/j.ijpvp.2012.05.005

Liyanage, K., & Dhar, A. S. (2018). Stresses in cast iron water mains subjected to non-uniform bedding and localised concentrated forces. *International Journal of Geotechnical Engineering*, *12*(4), 368–376. https://doi.org/10.1080/19386362.2017.-1282338

Liyanage, K. T. H., & Dhar, A. S. (2017). Effects of corrosion pits on wall stresses in cast-iron water mains. *Journal of Pipeline Systems Engineering and Practice*, *8*(4), 04017023. https://doi.org/10.1061/(asce)ps.1949-1204.0000286

Mondal, B. C., & Dhar, A. S. (2019). Burst pressure assessment of corroded pipelines using fracture mechanics criterion. *Engineering Failure Analysis*, *104*(August 2018), 139–153. https://doi.org/10.1016/j.engfailanal.2019.05.033

Montassir, S., Yakoubi, K., Moustabchir, H., Elkhalfi, A., Rajak, D. K., & Pruncu, C. I. (2020). Analysis of crack behaviour in pipeline system using FAD diagram based on numerical simulation under XFEM. *Applied Sciences (Switzerland)*, *10*(17). https://doi.org/10.3390/app10176129

Pachoud, A. J., Manso, P. A., & Schleiss, A. J. (2017). Stress intensity factors for axial semi-elliptical surface cracks and embedded elliptical cracks at longitudinal butt welded joints of steel-lined pressure tunnels and shafts considering weld shape. *Engineering Fracture Mechanics, 179*, 93–119. https://doi.org/10.1016/j.engfracmech.2017.04.024

Rajani, B., & Kleiner, Y. (2013). External and internal corrosion of large-diameter cast iron mains. *Journal of infrastructure systems*, *19*(4), 486-495.

Raju, I. S., & Newman, J. C. (1982). Stress-intensity factors for internal and external surface cracks in cylindrical vessels. *Journal of Pressure Vessel Technology, Transactions of the ASME, 104*(4), 293–298. https://doi.org/10.1115/1.3264220

Randeniya, C., Robert, D. J., Fu, G., & Li, C. Q. (2016). The effect of corrosion patch geometry on stress intensity factors for external surface cracks in cast iron water mains. *Proceedings of the 4th International Conference on Sustainable Construction Materials and Technologies (SCMT4), Nevada, United States, 7-11 August 2016*, pp. 1673-1680.

Turnbull, A. (2014). Corrosion pitting and environmentally assisted small crack growth. *Proceedings of the Royal Society A: Mathematical, Physical and Engineering Sciences, 470*(2169). https://doi.org/10.1098/rspa.2014.0254

USEPA. (2002). *Deteriorating Buried Infrastructure Management Challenges and Strategies. Environmental Protection Agency (EPA)*, 1–33. http://www.epa.gov/ogwdw/disinfection/tcr/pdfs/whitepaper_tcr_infrastructure.pdf

Wang, W., Zhou, A., Fu, G., Li, C. Q., Robert, D., & Mahmoodian, M. (2017). Evaluation of stress intensity factor for cast iron pipes with sharp corrosion pits. *Engineering Failure Analysis*, *81*, 254–269. https://doi.org/10.1016/j.engfailanal.2017.06.026

Wang, X., & Lambert, S. B. (1996). Stress intensity factors and weight functions for deep semi-elliptical surface cracks in finite-thickness plates. *International Journal of Pressure Vessels and Piping*, *65*, 75–87. https://doi.org/10.1046/j.1460-2695.2002.00502.x

Wasim, M., Li, C. Q., Robert, D., & Mahmoodian, M. (2020). Fracture toughness degradation of cast iron due to corrosive mediums. *International Journal of Pressure Vessels and Piping, 186(February)*, 104151. https://doi.org/10.1016/j.ijpvp.2020.-104151

Zhu, X. K., & Joyce, J. A. (2012). Review of fracture toughness (G, K, J, CTOD, CTOA) testing and standardization. *Engineering Fracture Mechanics, 85*, 1–46. https://doi.org/10.1016/j.engfracmech.2012.02.001

Chapter 4 Stress Intensity Factors for External Corrosions and Cracking of Buried Cast Iron Pipes

Atika Hossain Akhi, Ashutosh Sutra Dhar

Department of Civil Engineering, Memorial University of Newfoundland, St. John's, Newfoundland, CANADA

Abstract

The municipal water distribution systems across the world include a significant amount of cast-iron pipes. Many of the buried cast-iron pipes are over fifty years old and require rehabilitation. Municipalities decide on a rehabilitation solution between the replacement and re-use of the existing pipes based on the remaining strengths of the pipes. Fracture mechanics has appeared as the most viable tool for remaining strength assessment of the deteriorating pipes. However, a method of assessing the stress intensity factor (SIF) is often not available to the municipal engineers to apply the fracture mechanics. This paper presents a method for calculating the SIFs of buried cast iron pipes subjected to corrosion and crack on the exterior surface. Different semi-elliptical shaped defects were characterized using various aspect ratios (crack-depth to crack-length ratio) and relative depths (crack-depth to pipe thickness ratio). The SIFs were assessed for invert/crown and springline position cracks under internal pressure and vertical surface loads. A simplified method is proposed for evaluating the SIFs of buried pipes subjected to the exterior surface defects.

4.1 Introduction

Pipeline plays a significant role in the transportation of liquid and gas to meet the essential community needs. Water mains occupy a considerable portion of the pipeline systems. Cast iron pipelines in water mains were extensively used in the last century (USEPA, 2002). Some of these pipelines already exceeded their service life and are subjected to deterioration. Corrosions in buried pipelines are the most predominant causes of deterioration. Corrosions on the exterior surface (external corrosion) in buried cast iron pipes occur due to corrosive soils (Wasim et al., 2020). Corrosions on the interior surface (internal corrosions) are caused by water chemistry and flow characteristics (Rajani & Kleiner, 2012). The corroded pipelines are susceptible to leakage and breakage. Municipalities look for a strategy for rehabilitating the deteriorating pipes based on their remaining strengths. The conventional methods of assessing the remaining strength are based on the continuum mechanics theory where the pipe wall stresses are compared with the strength of pipe material (Liyanage & Dhar, 2018; Debnath et al., 2021). However, the continuum mechanics-based method cannot account for the stress singularity expected around the cracks in the corroded pipes. Fracture mechanics is considered suitable for examining crack initiation and propagation (Fahimi et al., 2016; Wang et al., 2017; Mondal & Dhar, 2019). The stress state around the crack tip is presented using the following parameters: Stress Intensity Factor (SIF), Strain Energy Release Rate (G), J-integral (J), and crack tip opening displacement (δ) of the material (Zhu & Joyce, 2012; Debnath et al., 2021). The limiting values of these parameters are termed as the fracture toughness. At a magnitude beyond the limiting value, a crack initiates and propagates. Stress intensity

factor and J-integral terms are used for brittle and ductile materials, respectively (Debnath & Dhar, 2019).

Cracks in pressure shells, such as pipelines, are often reported to have semi-elliptical shapes (Pachoud et al., 2017; Moustabchir et al., 2018; Montassir et al., 2020), which can occur in circumferential and longitudinal directions. Raju and Newman (1982) performed finite element analysis and developed an empirical equation to calculate the SIFs for semi-elliptical internal and external surface cracks. The empirical equation is based on different influence coefficients developed for various crack-depth to crack-length ratios (aspect ratios) ranging from 0.2 to 1.0 for in-air pipes. Wang and Lambert (1996) extended the study by performing three-dimensional (3D) finite element analysis (FEA) for the evaluation of SIFs at low aspect ratios (i.e., 0.05 and 0.1) with different depths of cracks (0.2, 0.5, and 0.8 times the wall thickness). SIFs for semi-elliptical external and internal surface cracks were calculated under constant, linear, quadratic, and cubic stress distributions on the cracked face. They calculated the weight functions for SIFs of surface and deepest cracks with low aspect ratio are within 5% of those given by Raju and Newman' equation. Li and Yang (2012) performed FEA to find SIFs with a high aspect ratio ($a/c > 1$) for semi-elliptical longitudinal internal cracks in cast iron pipes under internal pressure. The analysis was performed for crack-only defects with different aspect ratios and crack depths. The maximum SIF for surface crack with a high aspect ratio was found to occur at a similar location as that with a low aspect ratio. Fakkoussi et al. (2019) applied FEM and extended finite element model (XFEM) to determine SIFs for longitudinal semi-elliptical external cracks under internal pressure. It was found that SIFs

were significantly influenced by the locations of cracks in different longitudinal directions. Few other researchers also quantified SIFs for surface cracks of cast iron pipes under internal pressure (Zareei & Nabavi, 2016; Wang et al., 2017; Moustabchir et al., 2018). The authors performed the study under internal pressure for in-air pipe only. Cracks with corrosion were not considered.

Limited studies are available in the published literature on the evaluation of SIF for buried cast iron pipe considering soil pressure. Khoramishad and Ayatollahi (2009) evaluated the SIF of a semi-elliptical external crack for buried pipelines at different circumferential crack orientations. They found that the weight of soil has significant effects on SIF values. Randeniya et al. (2016) used 3D FEA for calculating the SIFs of external surface cracks in corroded cast iron pipes. Corrosion geometry was found to be an influencing factor on SIFs in cast-iron pipes. Recently, Debnath and Dhar (2019) performed FEA to observe the combined effect of internal pressure and surface load on SIF values for an external circular crack of buried pipes. The SIFs for buried pipes with various cracks and corrosions were not investigated.

This study evaluates the SIFs for the exterior semi-elliptical crack-only defects and cracks with corrosion defects of buried cast iron pipes. Three-dimensional FE analysis is performed with the external cracks for different aspect ratios and crack depths. The contour integral method is used to calculate SIFs at the invert/crown and springline positions of the pipe. Note that the SIFs for the crown and invert cracks are essentially the same for the loading conditions considered.

4.2 FE Modelling for External Defects

The commercial FE software, Abaqus/Standard (Dassault Systemes, 2014), was used for the analysis. The SIFs for in-air pipe with a crack-only defect were first investigated to validate the model with the available solution of Raju and Newman (1982). The validated in-air pipe model is used to investigate the SIFs for buried pipes. The study is then extended to investigate the buried pipes with a crack with corrosion defects. Figure 4.1 and Figure 4.2 show the crack-only defect and crack with corrosion defect on the exterior pipe surface considered in the current study.

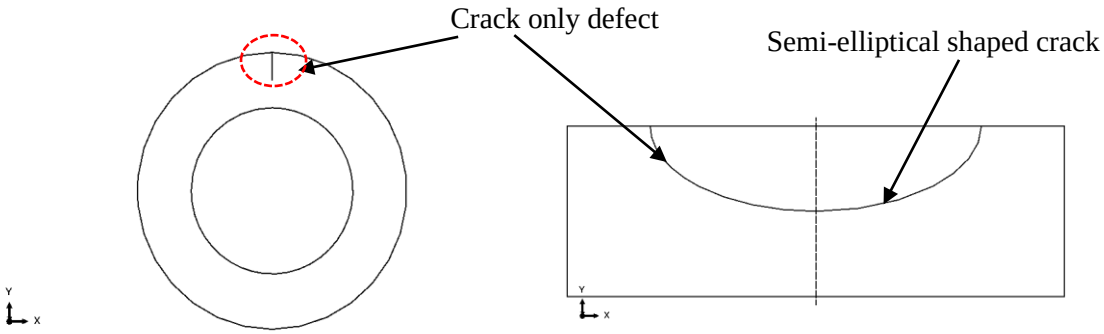

(a) Cross-section (b) Longitudinal section

Figure 4.1 External crack-only defect

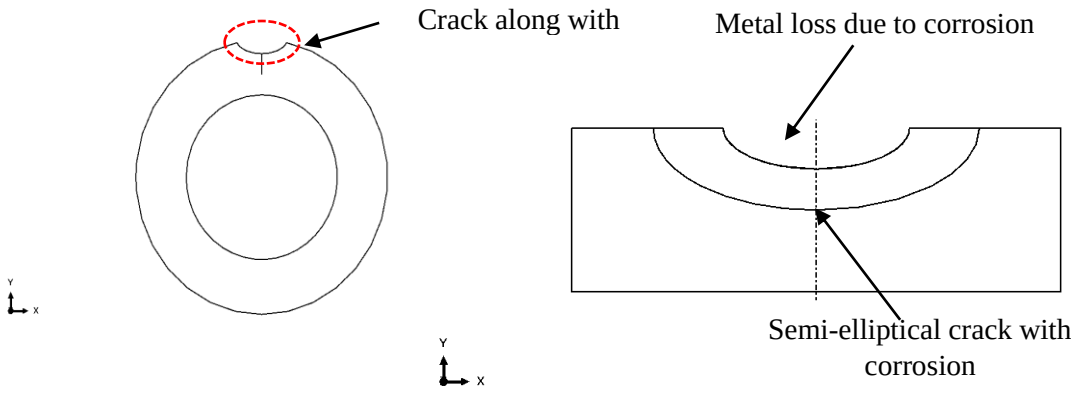

(a) Cross-section (b) Longitudinal section

Figure 4.2 External crack with corrosion defect

Raju and Newman (1982) proposed a simplified equation (Equation 4.1) based on extensive FE modeling for the calculation of Mode 1 SIF along the external semi-elliptical crack of a radially pressurized cylindrical vessel.

$$K_1 = \frac{PR}{t}\sqrt{\pi\frac{a}{Q}}F_e\left(\frac{a}{c},\frac{a}{t},\frac{t}{R},\varphi\right) \quad (4.1)$$

Where

K_1 = Mode 1 SIF

P = Radial internal pressure in the cylinder

R = Inner radius of the cylinder

t = Pipe wall thickness

$\frac{PR}{t}$ = Average hoop stress of an uncracked pipe subjected to internal pressure

a = Depth of the surface crack

Q = Shape factor for elliptical crack

F_e = Boundary-correction factor for external surface crack

c = Half-length of the surface crack

φ = Parametric angle of elliptical crack (Figure 4.3)

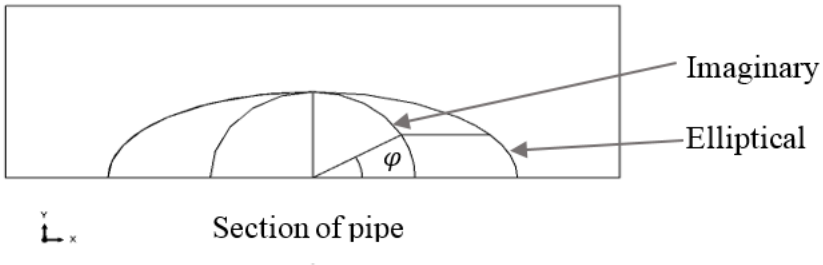

Figure 4.3 Parametric angle (φ) of semi-elliptical crack

The shape factor, *Q*, can be obtained from Equation 4.2 (Raju & Newman, 1982):

$$Q = 1 + 1.464(\frac{a}{c})^{1.65} \quad \text{For a} \leq \text{c} \tag{4.2}$$

The boundary-correction factor, F_e is expressed as in Equation 4.3 using influence coefficients for j^{th} (j=0,1,2,3) stress distribution on the crack surface (Raju & Newman, 1982):

$$F_e = \frac{t}{R}\left(\frac{R^2}{R_0^2 - R^2}\right)[2G_0 + 2\left(\frac{a}{R_0}\right)G_1 + 3(\frac{a}{R_0})^2 G_2 + 4(\frac{a}{R_0})^3 G_3] \tag{4.3}$$

Where,

R_0 = Outer radius of the cylinder

G_0, G_1, G_2, G_3 = Influence factors for four polynomial terms for uniform, linear, quadratic, and cubic distributions

Equations 4.1 to 4.3 were used to obtain the SIFs of different aspect ratios (*a/c*) with relative crack depths (*a/t*). The same *a/c* and *a/t* values were used in FE simulations. The SIFs obtained from the FE simulation and empirical equations were compared.

Table 4.1 shows the simulation parameters considered. The pipe has the outer diameter (D_o) of 220 mm and the wall thickness (*t*) of 10 mm. Material parameters of the cast iron (i.e. Young's modulus and Poisson's ratio) were obtained from test results by Debnath et al. (2021). Semi-elliptical defects of different *a/c* and *a/t* ratios were generated on the exterior wall. Similar parameters were used in a study of the SIFs for internal wall cracks in Akhi and Dhar (2021).

Table 4.1 Simulation parameters for pipe and external cracks

Parameters	**Value**
Young's Modulus, *E* (GPa)	125
Poisson's Ratio, ν	0.25
Density (gm/cm^3)	7.88
Internal Pressure (kPa)	600
Outer Diameter, D_0 (mm)	220
Inner Diameter, *D* (mm)	200
Relative Wall Thickness (*t/R*)	0.1
Aspect Ratios (*a/c*)	0.2, 0.4, 1.0
Relative Depths (*a/t*)	0.2, 0.5, 0.8

Pipe length was taken sufficiently long to avoid the boundary effects. Randeniya et al. (2016) observed that the effect of pipe length on SIFs is minimized for a ratio of the pipe length (L) to half-crack length (c) of greater than 20. Analyses were also conducted with various pipe lengths in the current study that confirm the finding of Randeniya et al. (2016). Therefore, $L/c > 20$ was used in all analyses presented here.

4.2.1 FE Model Development for Pipe with External Defects

The FE model of the pipe was developed in Abaqus module as a 3D deformable solid body. A crack is defined at prescribed location using a partition along the crack plane and assigning a seam on the plane so that the elements on both sides of the partition do not share nodes (not connected). The seam creates overlapping nodes to separate nodes on elements on each side of the crack or partition (Dassault Systemes, 2014). To define a semi-elliptical crack, a partition is made through extending a semi-elliptical shape around the pipe circumference using sweep technique in Abaqus (Figure 4.4). The crack plane and the crack front are then selected at the desired location. The crack tip is any point (nodal points) along the crack front (semi-elliptic boundary) where the contour integral is calculated. The contour integrals are calculated for layers of elements around the crack front perpendicular to the crack plane. Thus, the FE mesh with rings of elements surrounding the crack tip (the nodes on the crack front) is beneficial to define the contours. To develop circular contour, circular partition was created centering the crack front, extending over the whole length of the semi-elliptical crack (Figure 4.5). The partition also facilitates the generation of fine mesh to increase accuracy (Li & Yang, 2012; Randeniya et al., 2016). The singularity at

the crack tip in contour integral techniques is taken care of using either quadrilateral or linear brick elements with a collapsed side to induce wedge-shaped elements (Figure 4.5). Five contours resulted from the FE mesh are shown in Figure 4.6. The contours are automatically selected along the element boundaries across the crack front.

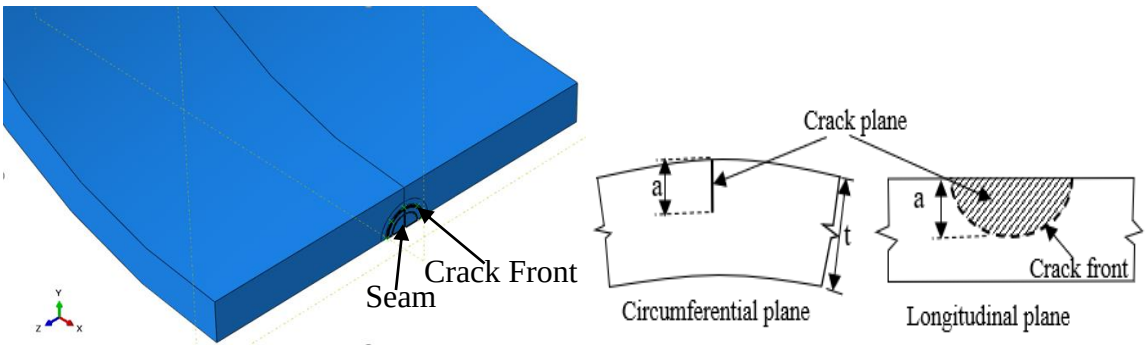

(a) 3D view (b) 2D view

Figure 4.4 Partitioning to define a semi-elliptical external crack

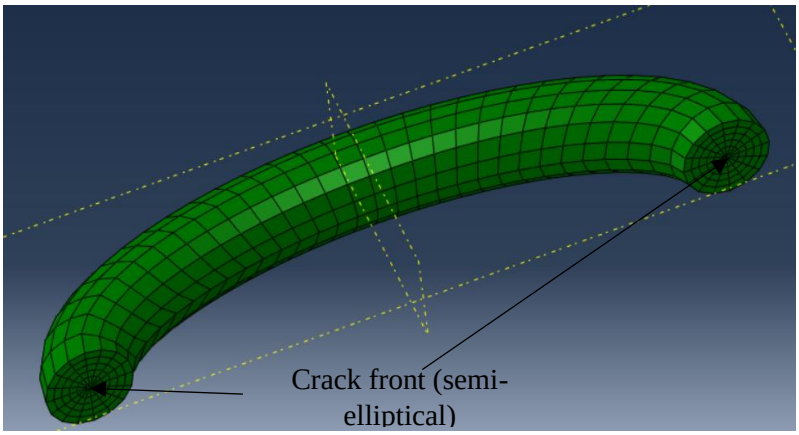

Figure 4.5 Partitioning to define circular element boundaries around the external crack front

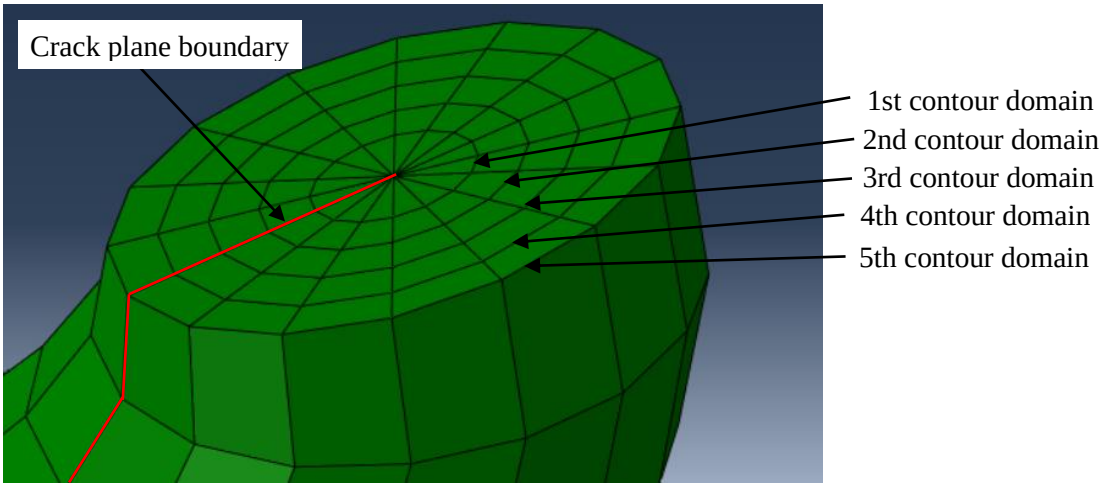

Figure 4.6 Five contours domain around the external crack

The virtual crack extension direction is specified normal to the crack front using *q*-vector in Abaqus (Dassault Systemes, 2014). The crack extension directions at each crack tip are different, which are defined for all crack tips along the crack front, editing the *q*-vector manually in the input data file. The resulting crack extension directions for the semi-elliptical crack are shown in Figure 4.7.

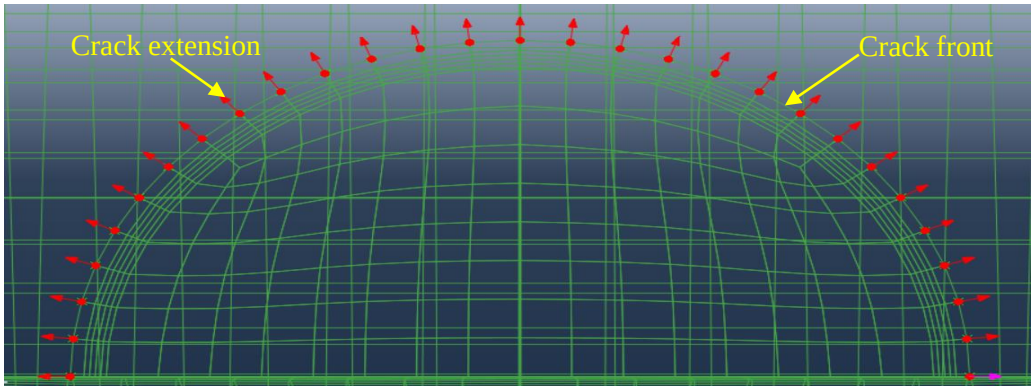

Figure 4.7 Crack extension direction of a semi-elliptical external crack

The higher-order twenty-nodded brick elements with reduced integration (C3D20R) and wedge element of C3D15 (15-node quadratic triangular prism element) and lower order eight-nodded linear brick elements (C3D8R) and wedge element of C3D6 (6-node linear triangular prism) are examined. No significant difference was observable in the results. Therefore, C3D6 wedge elements (around crack tips) with C3D8R were used in the analysis to save computational time. The mesh size dependency of the results was also minimized performing a mesh convergence study.

4.2.2 Validation of FE model for External Cracks

As the contour integral is path-independent, the SIFs obtained from each contour should be the same. The SIFs calculated at the crack edge (φ = 0°or φ = 180°) from contours 2 to 5 are plotted in Figure 4.8. The first contour usually provides abrupt results due to the effects of singularity (Dassault Systemes, 2014) and, therefore, not considered. Figure 4.8 shows that the SIFs along each of the contours are the same, validating the FE model.

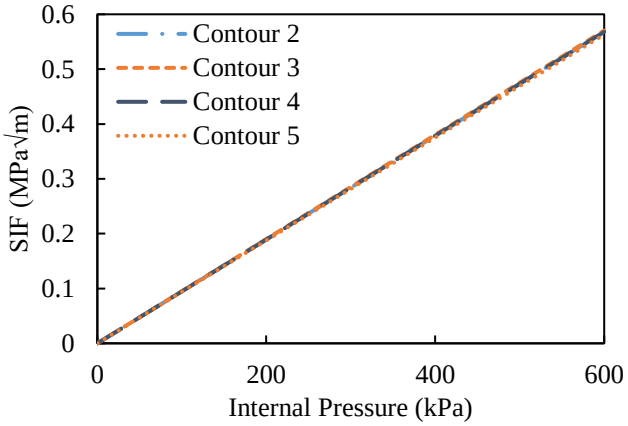

Figure 4.8 SIF for four contours (φ = 0° or φ = 180°)

The results of FE analysis were also compared with the SIFs obtained from the semi-empirical equation of Raju and Newman (1982) for further validation. Figure 4.9 shows the comparison of SIFs at the internal pressure of 600 kPa for various *a/c* and *a/t*. The comparisons are presented for crack-only defects on the exterior surface of in-air pipes. No significant difference between the SIFs calculated using the FE model and the semi-empirical equation is observed in the figure. The maximum difference is seen for *a/t* = 0.8 for all aspect ratios, which is less than 5%. A similar difference (< 5%) of FE calculations from the semi-empirical equation was reported earlier in Randeniya et al. (2016) and Debnath and Dhar (2019) for *a/c* = 1.

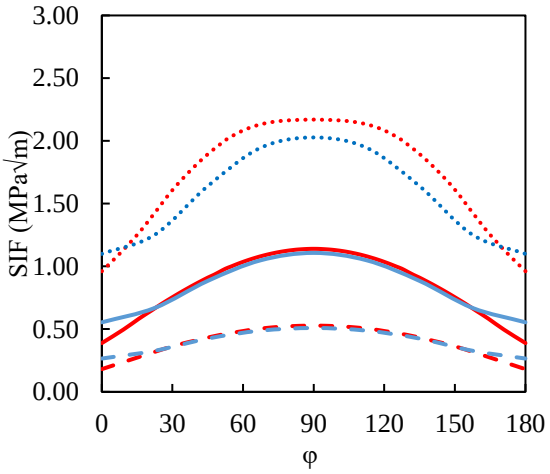

(a) *a/c*=0.2

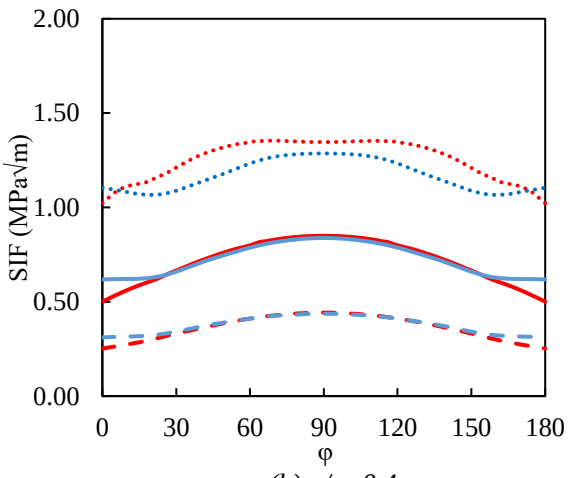

(b) a/c=0.4

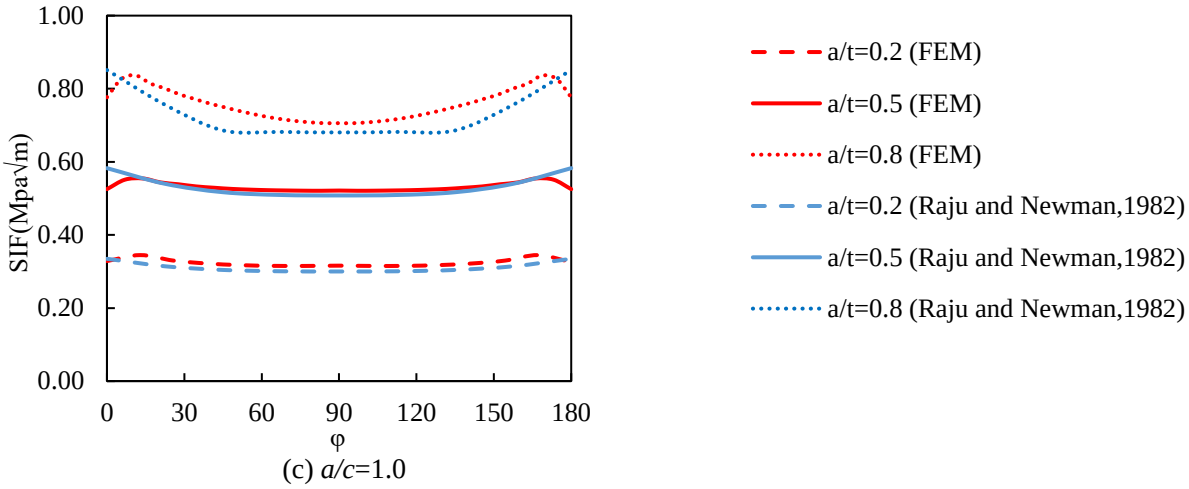

(c) *a/c*=1.0

Figure 4.9 Comparison of SIFs from FEM of external crack and Raju and Newman (1982)

Figure 4.9 shows that SIFs are decreasing with increasing *a/c*. The highest SIF was observed at the center of the crack (i.e., $\varphi = 90°$) for *a/c* = 0.2 and *a/c* = 0.4. Thus, the crack might propagate from the center point for the lower *a/c* (0.2 and 0.4) that would increase the crack depth. The SIFs are higher at the edge ($\varphi = 90°, 180°$) for circular crack (*a/c* =1), indicating that the crack propagation would be from the edge that might increase the crack length. A similar observation was reported for the internal crack of cast iron pipe in Akhi and Dhar (2021).

4.2.3 FE Model for Buried Pipeline with External Defects

The pipe model described in the previous section was considered for soil-pipe interaction analysis. The surrounding soil was assumed as 3D deformable-body. The soil was characterized as an elastic-perfectly plastic material and defined by the Mohr-Coulomb failure criteria due to simplicity, reasonable computational time, and the high level of understanding among the engineers (Robert et al., 2015). Soil properties typical for

medium dense sand were used, presented in Table 4.2. A small cohesion of the sand was used to ensure numerical stability. The general contact algorithm available in Abaqus was used for modeling the soil-pipe interface. The master and slave surfaces in the general contact algorithm are automatically selected. The friction coefficient (μ) between the soil and the pipe was assumed to be 0.30 to simulate Columb friction model. However, the friction parameters were expected to have an insignificant contribution to the SIF under the loading conditions considered (Fu et al., 2020).

Table 4.2 Typical parameters for medium dense sand

Material Properties	**Soil**
Density (gm/cm^3)	1.77
Young's Modulus (MPa)	24
Poisson's Ratio	0.25
Friction Angle in (°)	38
Dilation Angle in (°)	8
Cohesion (kPa)	0.1

Figure 4.10 shows the FE model used for soil pipe interaction analysis. The pipe was placed at the center of the model, maintaining a larger distance (~10D) from the boundary to avoid the boundary effects. The length of the FE model was selected, ensuring $L/c > 20$. The SIFs were calculated at two crack locations of crack such as crown/invert and springline.

The boundary conditions are selected to restrain the bottom boundary from any movement. The side boundaries are provided with roller support to restrain any lateral movement. Half of the soil-pipe system with the symmetric boundary condition was considered for the springline crack to take advantage of symmetry for saving computational time. Thus, the pipe cross-section is assumed as symmetric about a diametric plane, which essentially indicates a pipe with two diametrically opposite position cracks. Since the SIF for a particular crack is not affected by any other crack located at sufficient distance, the results are not expected to be affected by the assumption of the symmetric condition. Symmetric boundary conditions were applied on the planes of symmetry.

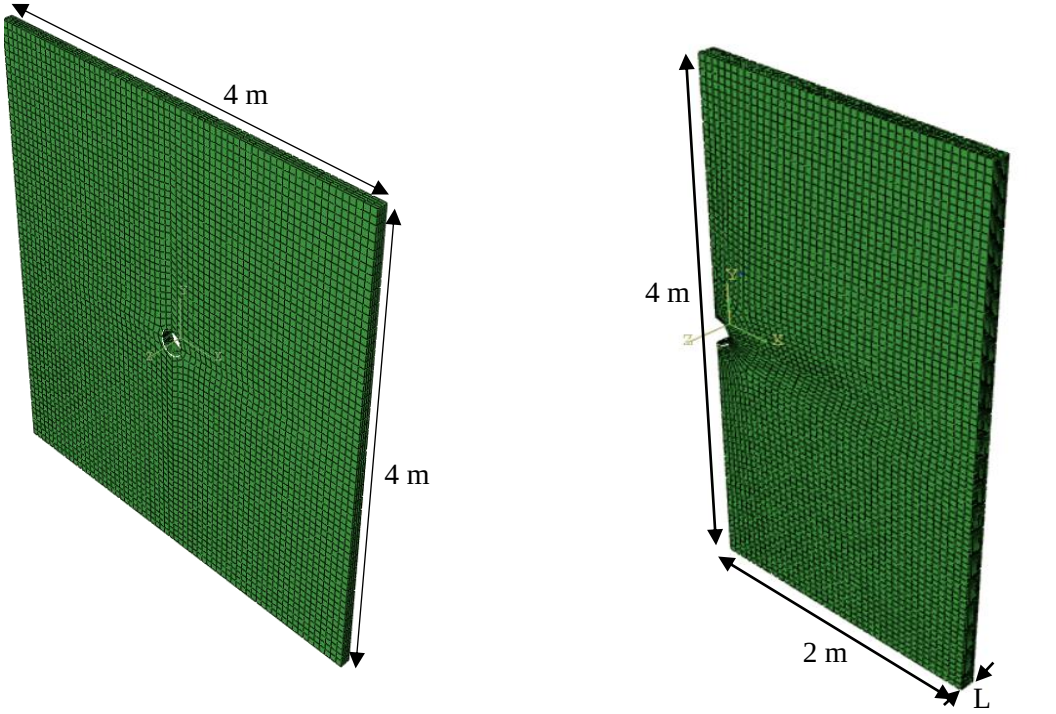

(a) Crown/invert crack analysis

(b) Springline crack analysis

Figure 4.10 FE model of external crack for soil-pipe interaction analysis

FE analysis was performed in two steps to obtain the SIFs. In the first step, 600 kPa internal pressure was applied inside the pipe. In the second step, an additional surface load equivalent to the weight of 2 m of soil (34.73 kPa) was applied at the top boundary. The SIFs due to the combined load were compared with those due to the internal pressure to identify the effects of the surface load.

4.3 Results

4.3.1 Buried Pipes with External Crack Only Defects

The focus of the current study is to evaluate the SIFs for corrosions and cracks on the exterior surface of buried cast iron pipe subjected to internal pressure and surface load. The orientation of the semi-elliptical crack is an essential consideration for the critical SIFs. Analysis was first performed to calculate SIFs for longitudinal and circumferential cracks. The results showed that SIFs were much higher for longitudinal cracks than the circumferential cracks under the loading conditions considered (internal pressure and vertical surface load). Therefore, the longitudinal crack was considered for further analysis.

The SIFs for a longitudinal external crack with various aspect ratios (a/c = 0.2, 0.4 and 1) and crack depths (a/t = 0.2, 0.5 and 0.8) are plotted in Figure 4.11 and 4.12. Figure 4.11 presents the SIFs for springline cracks, and Figure 4.12 presents the SIFs for crown/invert cracks. The SIFs due to the internal pressure are also included in the figures. Figure 4.11 shows that the SIFs for the springline crack increase by the application of surface load from those with only the internal pressure. The increase in tensile (bending) stress at the springline due to the surface load is the cause of the increased SIFs. The SIFs

are higher for deeper cracks (higher *a/t*) and lower for higher aspect ratios (*a/c*). The maximum SIFs are noticed at the center of the crack for lower crack depths and aspect ratios. The SIF at the crack center is responsible for increasing the crack depth. For deeper cracks (e.g., *a/t* = 0.8), the SIFs are less at the center and increase at the edge, particularly for higher aspect ratio (e.g., *a/c* = 1). For *a/c* = 1.0 (circular crack) and *a/t* = 0.8, the SIF due to the combined load is reduced at the crack's center and is less than the SIF due to the internal pressure. The location of the highest SIF moved from the center for the internal pressure to the edge for the combined load. The high SIF at the crack edge, if higher than the fracture toughness, can increase the crack length.

The SIFs of the crown/invert crack for the application of surface load decrease (Figure 4.12) due to the compressive bending stress on the outer surface of the pipe. The maximum SIFs for the crown/invert cracks are located at the center of the crack for the buried pipe. The SIFs are higher for higher *a/c*.

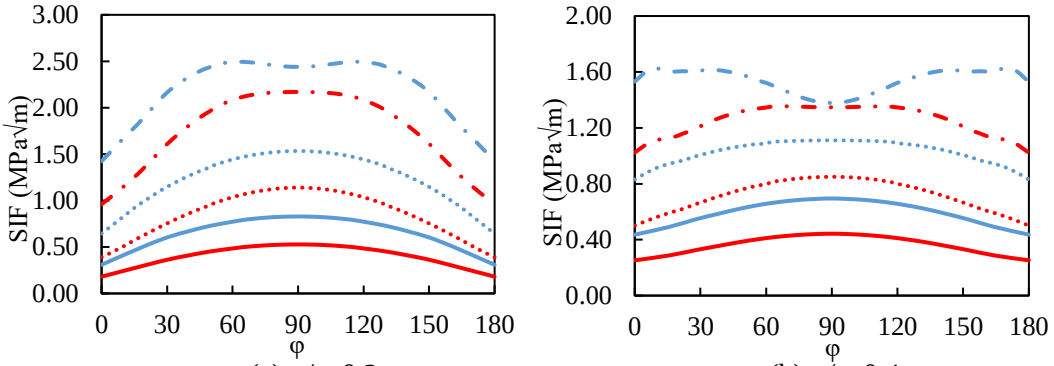

(a) *a/c*=0.2 (b) *a/c*=0.4

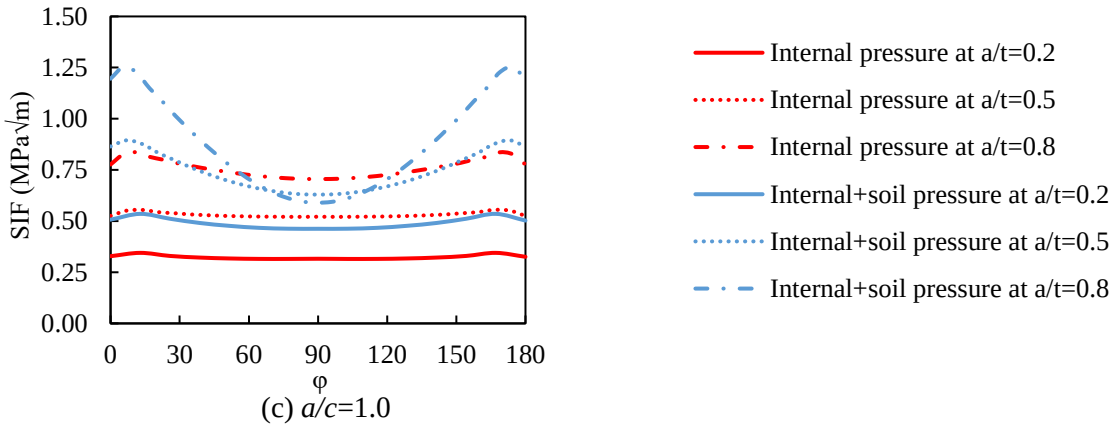

(c) *a*/*c*=1.0

Figure 4.11 SIFs for the external springline crack of a buried pipe

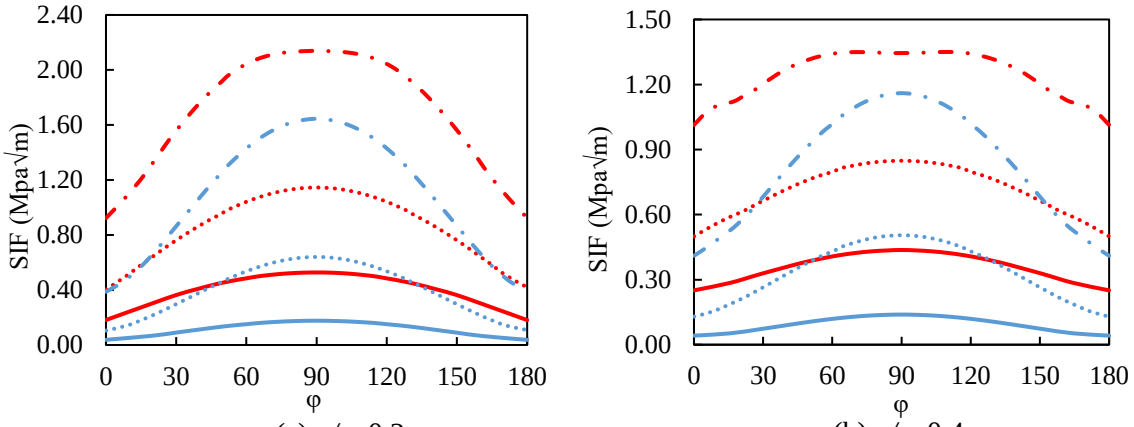

(a) *a*/*c*=0.2

(b) *a*/*c*=0.4

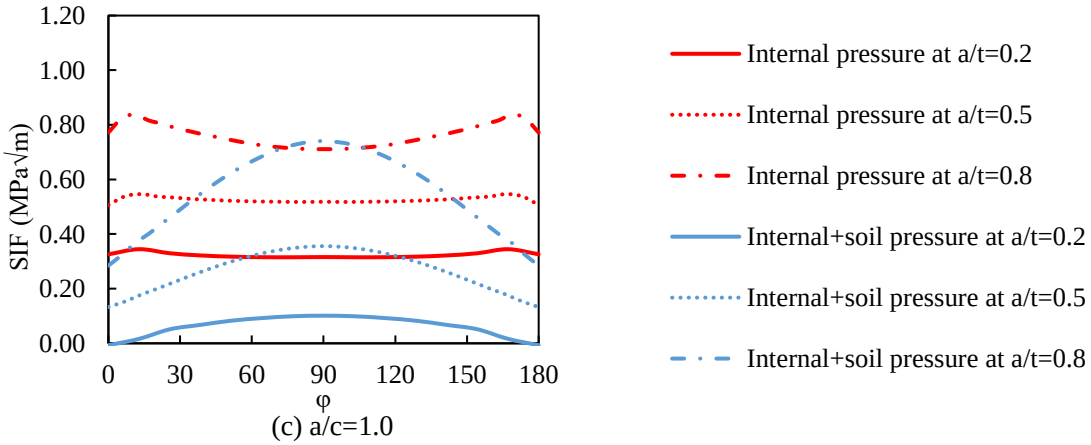

(c) a/c=1.0

Figure 4.12 SIFs for external invert/crown crack of a buried pipe

Figure 4.13 compares the SIFs under internal pressure for the buried pipe and those for the in-air-pipe obtained from the equation of Raju and Newman (1982). The comparison illustrates a negligible difference between the SIFs for the in-air pipe and the buried pipe. Thus, the SIF due to internal pressure for buried pipe can reasonably be calculated using the equation of Raju and Newman (1982). The contribution of surface load on the SIF can then be added to obtain the SIF due to the combined load, as in Equation 4.4.

$$K_{total} = K_{pressure} + K_{surface} \tag{4.4}$$

Where,

K_{total} = Total SIF due to combined load

$K_{pressure}$ = SIF due to internal pressure

$K_{surface}$ = SIF due to surface load

The $K_{pressure}$ can be calculated using the equation of Raju and Newman (1982). A simplified method is developed in the present study for calculating $K_{surface}$ based on a FE investigation (discussed later).

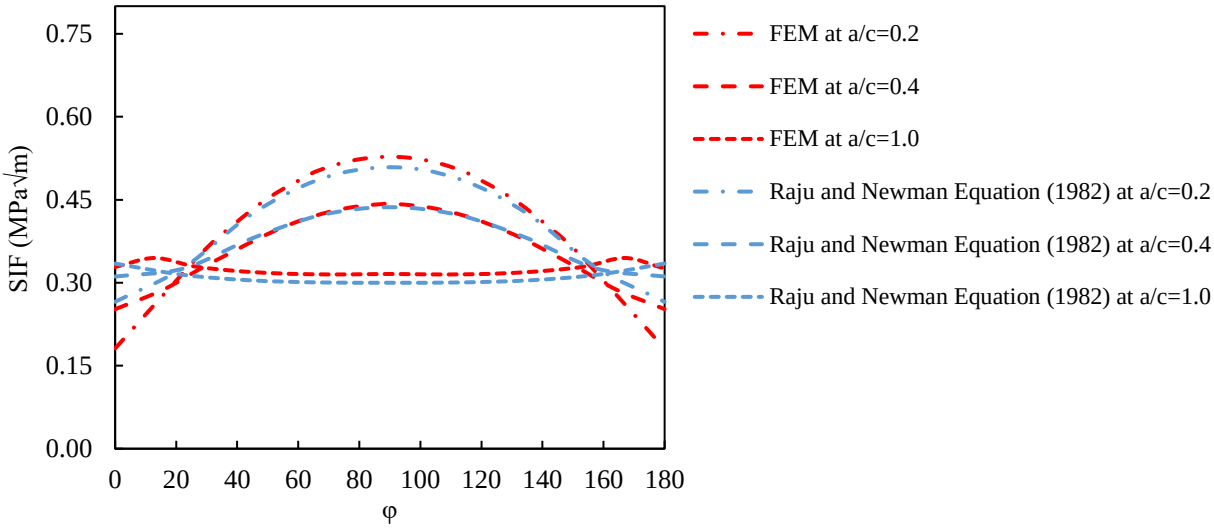

Figure 4.13 SIFs for external cracks due to internal pressure for in-air and buried pipes

4.3.2 Buried Pipe with External Crack-with-Corrosion Defects

SIFs for a crack with corrosion defect of a buried pipe were investigated considering half ellipsoidal shape of corrosion, shown in Figure 4.14, for different aspect ratios. The location of the crack in the corroded pipe is first identified through analysis using the Extended Finite Element Method (XFEM). Figure 4.14(b) shows the location of a crack in the corrosion obtained from XFEM analysis. A crack was applied at this location to calculate the SIFs. A corrosion depth of 3 mm and a crack depth of 2 mm were assumed to constitute the total defect depth as 5.00 mm. It resulted in the *a/t* as 0.5 for the pipe with a wall thickness of 10 mm.

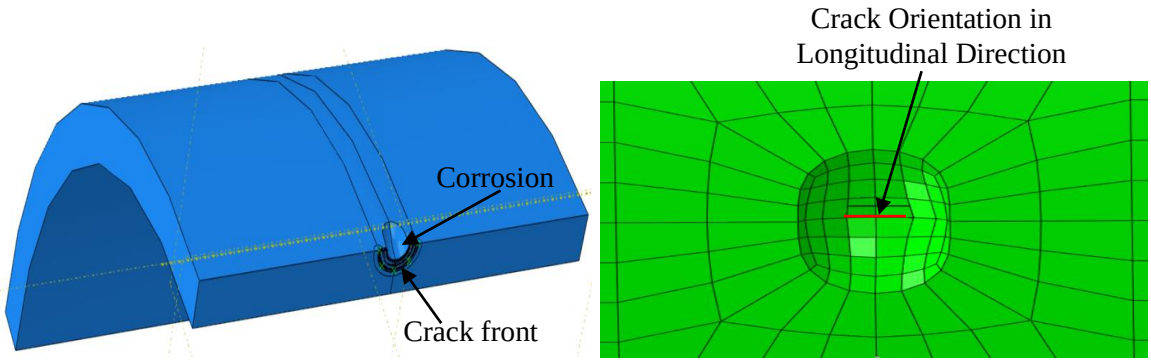

(a) Corrosion and crack (b) Crack location from XFEM analysis

Figure 4.14 An external crack with a semi-ellipsoidal corrosion defect

SIFs calculated for crack only and crack with corrosion defects are presented in Figure 4.15 for the springline and invert/crown cracks. The depth of the crack-only defect was the same as the total depth of the crack with corrosion defect (i.e., 5 mm). The crack length was taken the same in both cases. Figure 4.15 shows that the SIFs are almost the same for the crack-with-corrosion defect as those for the crack-only defect having the depth same as the total depth of corrosion and crack. Thus, the solution developed for crack-only defect can be applied for crack-with corrosion defect using the total depth of the defect.

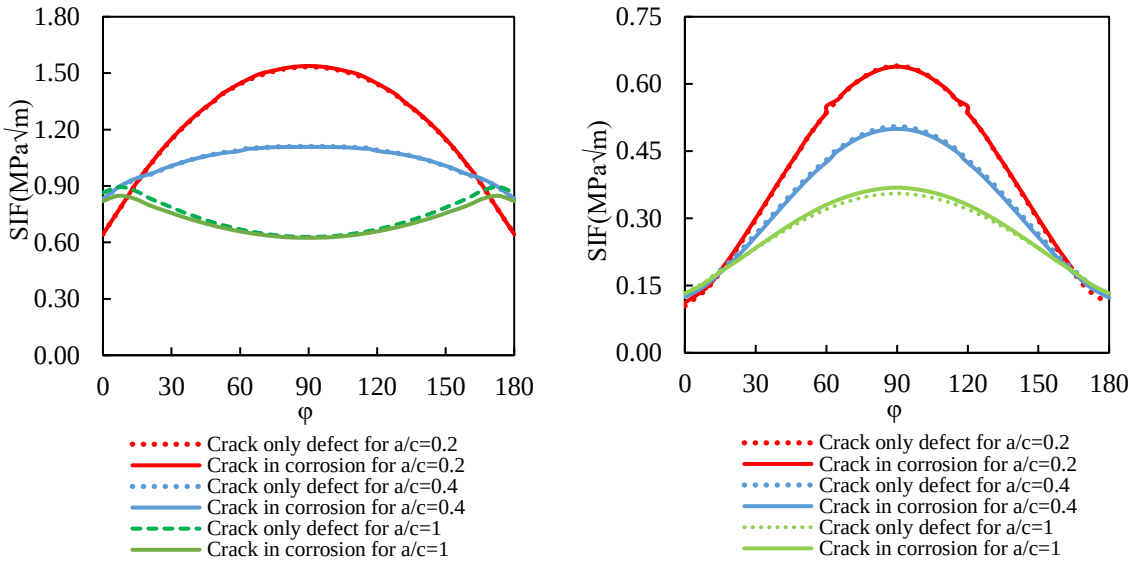

(a) Springline crack (b) Invert crack

Figure 4.15 SIF for external crack only and crack with corrosion defects for *a/t* = 0.5

4.3.3 SIFs for External Crack due to Surface Load

Debnath and Dhar (2019) employed a simplified equation for the calculation of SIF due to surface load for a circular crack in the buried pipeline Equation 4.5.

$$K_{surface} = q\sqrt{\pi \frac{a}{Q}} F_s\left(\frac{a}{c}, \frac{a}{t}, \frac{t}{R}, \varphi\right) \tag{4.5}$$

Here,

q = surface load. The surface load was applied to simulate the gravity load calculated as $q = \rho g h$ where ρ, g and h are density, acceleration due to gravity, and depth of soil cover, respectively.

F_s = Influence coefficient, which is a function of *a/c*, *a/t*, *t/R* and φ.

Q = Shape parameter

Ichsan (1994) recommended the shape parameter, Q as follows:

$$Q = 1 + 1.464\left(\frac{a}{c}\right)^{1.65} \qquad for\ \frac{a}{c} \leq 1 \tag{4.6}$$

$$Q = 1 + 1.464\left(\frac{c}{a}\right)^{1.65} \qquad for\ \frac{c}{a} \leq 1 \tag{4.7}$$

The influence factor, F_s, for semi-ellipteical cracks was developed in the current study for using Equation 4.5 to calculate the SIFs. Based on the SIFs obtained from FE analysis, the $K_{surface}$ was calculated using Equation 4.4. The influence coefficients for the surface loads for semi-elliptical external surface cracks were then back-calculated using Equation 4.5. The influence coefficients, F_s for different aspect ratios (a/c = 0.2, 0.4, 1.0) and relative depths (a/t = 0.2, 0.5, 0.8) for different parametric angles are presented in Table 4.3. As seen in the table, the influence coefficient is positive for springline crack and negative for invert crack, indicating an adverse effect of surface load on the springline crack. The influence factors proposed in Table 4.3 can be used for calculating SIFs for crack only and crack with corrosion defects (with a total depth of defect).

Table 4.3 Influence coefficients for external surface cracks

a/c	Crack depth	Springline			Invert		
		a/t			*a/t*		
	Angle	**0.2**	**0.5**	**0.8**	**0.2**	**0.5**	**0.8**
0.2	0	48.72	61.77	88.19	-54.95	-71.85	-102.21
	π/8	82.59	90.35	104.81	-93.50	-105.57	-128.54
	π/4	102.53	98.31	95.42	-118.07	-119.05	-129.11
	3π/4	112.19	97.07	68.23	-130.37	-122.14	-109.09
	π/2	114.80	95.06	51.38	-133.94	-121.86	-94.27
0.4	0	76.97	92.75	106.02	-87.55	-104.94	-126.10
	π/8	89.34	91.81	92.67	-102.24	-106.17	-116.55
	π/4	98.95	84.33	61.15	-115.16	-102.54	-89.80
	3π/4	104.08	74.10	24.80	-122.50	-95.13	-56.11
	π/2	105.74	69.14	6.59	-124.94	-91.12	-38.66
1.0	0	101.75	122.37	119.49	-189.87	-134.71	-138.86
	π/8	104.92	101.58	80.88	-165.74	-118.74	-103.84
	π/4	93.65	69.22	24.02	-139.33	-87.82	-47.91
	3π/4	85.96	47.16	-17.38	-126.09	-66.31	-6.98
	π/2	83.55	39.03	-33.04	-122.43	-58.55	8.41

Figure 4.16 presents the influence factors for the springline and invert/crown cracks with different aspect ratios. The figure shows positive influence factors for the springline crack and negative factors for the invert/crown cracks. However, the magnitudes depend

significantly on the aspect ratios and the crack depths. The magnitudes of F_s in Figure 4.16 can be used to calculate the change in the SIF due to surface load using Equation 4.5.

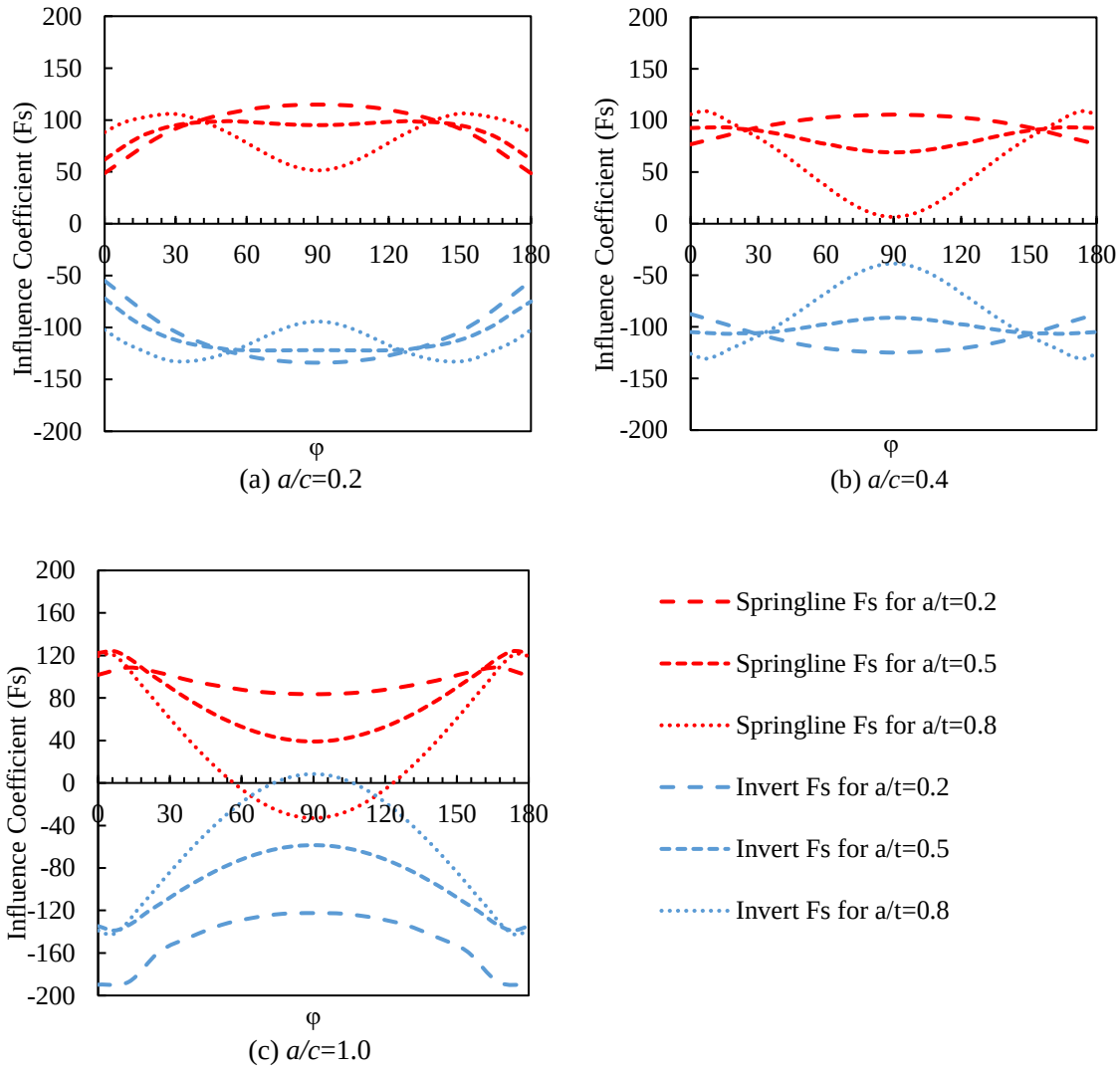

Figure 4.16 Influence factors for external invert and springline crack

4.4 Conclusions

In this study, the stress intensity factors (SIF) were investigated using FE analysis for semi-elliptical defects on the external surface of buried cast iron pipes. The SIFs were

evaluated for crack only and crack with corrosion defects under internal pressure and vertical surface load. The defects were simulated for different aspect ratios (*a/c*) and relative crack depths (*a/t*). The findings from the study are as follows:

- The longitudinally oriented external surface crack was critical for buried pipe in uniform ground subjected to internal pressure and surface load.
- There was no effect of the surrounding soil on the SIFs of buried pipe subjected to the internal pressure. Raju and Newman (1982) equation for in-air pipes can be used for buried pipes to calculate the SIFs due to internal pressure.
- The surface load increased the SIFs for springline cracks due to tensile bending stress in the exterior pipe wall and decreased the SIFs for invert/crown cracks due to compressive bending stress. The SIFs due to the combined load (internal pressure and surface load) can be obtained by adding the contribution of the surface load to the SIFs due to internal pressure. New influence coefficients were proposed for calculating SIFs under surface load using a simplified equation.
- The SIFs for crack with corrosion defect were essentially the same as the SIFs for crack only defect with the crack depth equal to the sum of the crack depth and the corrosion depth. Thus, the solution developed for the crack-only defect can be used for the analysis of cracks with corrosion defects.
- The maximum SIF was located at the crack's center for low aspect ratios (low *a/c*) and high crack depths. For a high aspect ratio or circular springline crack, the SIF was higher near the crack's edge. The SIF at the crack center would increase the

depth, while the SIF at the crack edge would increase the crack length if the SIF exceeds the fracture toughness.

- Parameters *a/c* and *a/t* significantly affected the influence coefficients for the SIF due to surface load.

4.5 References

Akhi, A. H., & Dhar, A. S. (2021). Fracture parameters for buried cast iron pipes subjected to internal corrosions. *Journal of Pipeline Science and Engineering* (Submitted).

Dassault Systemes. (2014). *ABAQUS/CAE user's guide*. Dassault Systemes Simulia Corp. Providence, RI, USA.

Debnath, S., Ali, I. M., Dhar, A. S., & Thodi, P. N. (2021). Material properties for fracture mechanics based strength assessment of cast iron water mains. *Canadian Journal of Civil Engineering*, *48(1)*, 1–47. https://doi.org/10.1139/cjce-2019-0229

Debnath, S., & Dhar, A. S. (2019). Assessment of stress intensity factor for buried cast iron pipeline using finite element analysis. *72nd Canadian Geotechnical Conference (GeoSt.John's 2019), St. John's, NL, Canada. September 29 - October 2, 2019.*

Fakkoussi, S. E. I., Moustabchir, H., Elkhalfi, A., & Pruncu, C. I. (2019). Computation of the stress intensity factor KI for external longitudinal semi-elliptic cracks in the pipelines by FEM and XFEM methods. *International Journal on Interactive Design and Manufacturing*, *13(2)*, 545–555. https://doi.org/10.1007/s12008-018-0517-1

Fahimi, A., Evans, T. S., Farrow, J., Jesson, D. A., Mulheron, M. J., & Smith, P. A. (2016). On the residual strength of aging cast iron trunk mains: Physically-based models for asset failure. *Materials Science and Engineering A, 663*, 204–212. https://doi.org-/10.1016/j.msea.2016.03.029

Fu, G., Zhang, C., Deo, R., Rathnayaka, S., Shannon, B., & Kodikara, J. (2020). A model of stress concentration factors for external corrosion patches on large-diameter underground cast iron pipes. *Sustainable and Resilient Infrastructure*, *00*(00), 1–12. https://doi.org/10.1080/23789689.2020.1828022

Ichsan, S. P. (1994). Fatigue crack growth predictions of surface cracks under constant-amplitude and variable-amplitude loading. *Delft University of Technology, Faculty of Aerospace Engineering*.

Khoramishad, H., & Ayatollahi, M. R. (2009). Finite element analysis of a semi-elliptical external crack in a buried pipe. *Transactions of the Canadian Society for Mechanical Engineering, 33(3),* 399–409. https://doi.org/10.1139/tcsme-2009-0028

Li, C. Q., & Yang, S. T. (2012). Stress intensity factors for high aspect ratio semi-elliptical internal surface cracks in pipes. *International Journal of Pressure Vessels and Piping, 96–97*, 13–23. https://doi.org/10.1016/j.ijpvp.2012.05.005

Liyanage, K., & Dhar, A. S. (2018). Stresses in cast iron water mains subjected to non-uniform bedding and localised concentrated forces. *International Journal of Geotechnical Engineering, 12(4),* 368–376. https://doi.org/10.1080/19386362.2017.-1282338

Mondal, B. C., & Dhar, A. S. (2019). Burst pressure assessment of corroded pipelines using fracture mechanics criterion. *Engineering Failure Analysis, 104(August 2018)*, 139–153. https://doi.org/10.1016/j.engfailanal.2019.05.033

Montassir, S., Yakoubi, K., Moustabchir, H., Elkhalfi, A., Rajak, D. K., & Pruncu, C. I. (2020). Analysis of crack behaviour in pipeline system using FAD diagram based on numerical simulation under XFEM. *Applied Sciences (Switzerland), 10(17)*. https://doi.org/10.3390/app10176129

Moustabchir, H., Arbaoui, J., Azari, Z., Hariri, S., & Pruncu, C. I. (2018). Experimental/numerical investigation of mechanical behaviour of internally pressurized cylindrical shells with external longitudinal and circumferential semi-elliptical defects. *Alexandria Engineering Journal, 57(3)*, 1339–1347. https://doi.org/10.1016/j.aej.2017.05.022

Pachoud, A. J., Manso, P. A., & Schleiss, A. J. (2017). Stress intensity factors for axial semi-elliptical surface cracks and embedded elliptical cracks at longitudinal butt welded joints of steel-lined pressure tunnels and shafts considering weld shape. *Engineering Fracture Mechanics, 179*, 93–119. https://doi.org/10.1016/j.engfracmech.2017.04.024

Rajani, B., & Kleiner, Y. (2012). Fatigue failure of large-diameter cast iron mains. *Water Distribution Systems Analysis 2010 - Proceedings of the 12th International Conference, WDSA 2010, 1926*, 1146–1159. https://doi.org/10.1061/41203(425)104

Raju, I. S., & Newman, J. C. (1982). Stress-intensity factors for internal and external surface cracks in cylindrical vessels. *Journal of Pressure Vessel Technology, Transactions of the ASME, 104(4)*, 293–298. https://doi.org/10.1115/1.3264220

Randeniya, C., Robert, D. J., Fu, G., & Li, C. Q. (2016). The effect of corrosion patch geometry on stress intensity factors for external surface cracks in cast iron water mains. *Sustainable Construction Materials and Technologies*, 2016-August.

Robert, D. J., Soga, K., & Britto, A. M. (2015). Soil constitutive models to simulate pipeline-soil interaction behaviour. In *International Conference on Geotechnical Engineering ICGE Colombo* (pp. 347-350).

USEPA. (2002). Deteriorating Buried Infrastructure Management Challenges and Strategies. *Environmental Protection Agency (EPA)*, 1–33. http://www.epa.gov/og-wdw/disinfection/tcr/pdfs/whitepaper_tcr_infrastructure.pdf

Wang, W., Zhou, A., Fu, G., Li, C. Q., Robert, D., & Mahmoodian, M. (2017). Evaluation of stress intensity factor for cast iron pipes with sharp corrosion pits. *Engineering Failure Analysis*, *81*, 254–269. https://doi.org/10.1016/j.engfailanal.2017.06.026

Wang, X., & Lambert, S. B. (1996). Stress intensity factors and weight functions for deep semi-elliptical surface cracks in finite-thickness plates. *International Journal of Pressure Vessels and Piping*, *65*, 75–87. https://doi.org/10.1046/j.14602695.-2002.00502.x

Wasim, M., Li, C. Q., Robert, D., & Mahmoodian, M. (2020). Fracture toughness degradation of cast iron due to corrosive mediums. *International Journal of Pressure*

Vessels and Piping, 186(February), 104151. https://doi.org/10.1016/j.ijpvp.2020.-104151

Zareei, A., & Nabavi, S. M. (2016). Calculation of stress intensity factors for circumferential semi-elliptical cracks with high aspect ratio in pipes. *International Journal of Pressure Vessels and Piping, 146*, 32–38. https://doi.org/10.-1016/j.ijpvp.2016.05.008

Zhu, X. K., & Joyce, J. A. (2012). Review of fracture toughness (G, K, J, CTOD, CTOA) testing and standardization. *Engineering Fracture Mechanics, 85*, 1–46. https://doi.org/10.1016/j.engfracmech.2012.02.001

Chapter 5 Conclusions and Recommendations

5.1 Conclusions

Cast iron pipes are an essential infrastructure of the municipal water supply system. The leakage and breakage of the cast iron pipes are frequently occurring in different municipalities. Different socio-economic and environmental problems are associated with pipeline failures. Municipalities all around the world need to find out economical option between the replacement and re-use of the existing pipes. Pipeline failures are assessed based on the loss of strength of wall stress and loss of toughness. The strength-based conventional method has some limitations in capturing the stress singularity expected for corroded and/or cracked pipes. The fracture mechanics can successfully overcome the limitation of the conventional method and can capture the crack initiation and propagation. In fracture mechanics, the strength of the material against cracking is evaluated using Stress Intensity Factor (SIF), Strain Energy Release Rate (G), J-integral (J) for brittle material. This research focuses on developing a method for calculating SIFs for semi-elliptical internal and external surface defects of buried cast iron pipes. The SIFs were determined for crack only and crack with corrosion defects subjected to internal pressure and surface load. The analysis was conducted on crown/invert and springline position defects.

5.1.1 Method for Calculating SIFs

The fracture mechanics was implemented in this study to evaluate the SIFs for internal and external surface defects (crack only and crack with corrosion) of buried cast iron pipe. The static implicit algorithm in FE program, Abaqus was performed. The current

study employs the contour-integral method for calculating stress intensity factors. Numerical modeling technique to perform the analysis was developed, including partitioning the model for assignment of crack, creating seam to separate the sharing of nodes, and defining the crack, crack front, and crack extension direction. The tubular section centering the crack front was partitioned through the perimeter of the crack to facilitate the fine meshing around the crack front/tips and defining the contours. The singularity at the crack tip in contour integral techniques was ensured using linear brick elements (C3D8R) with wedge element of C3D6 (6-node linear triangular prism). The crack extension direction was kept perpendicular to the crack front along the crack tip. The five contours, assigned to obtain path-independent SIFs, are automatically selected in Abaqus. The SIFs of in-air pipe were compared with Raju and Newman (1982) equation for validation of the modeling technique. The in-air pipe model was considered for soil-pipe interaction analysis. The SIFs for a crack with corrosion defect for a buried water main was calculated considering the half ellipsoidal shape of corrosion. Finding from this research are summarized as follow.

5.1.2 Major Findings

- The longitudinal crack on the internal and external surface of buried pipes is the most critical under internal pressure and surface loads.
- The presence of surrounding soil without the surface load does not influence the SIFs for both internal and external surface cracks under the internal pressure

loading. Thus, the SIFs of in-air pipe from the equation of Raju and Newman (1982) can be used for buried pipes under internal pressure loading.

- The compressive bending stress due to the surface load reduces the SIFs of springline crack in the interior pipe wall and increases the SIFs for invert/crown cracks due to tensile bending stress. An opposite mechanism was observed for external surface defects where the SIFs increases for the springline crack and decreases for the invert/crown cracks. The SIFs of Raju and Newman (1982) for internal pressure can be added to the contribution of surface load to obtain the SIFs due to combined load for both surface cracks. New influence coefficients of internal and external surface cracks are proposed for calculating SIFs under surface load.
- The crack only and crack on corrosion defects can be treated as the same for calculating SIF using the same defect depth (sum of crack depth and corrosion depth). This statement is true for external and internal surface semi-elliptical cracks.
- For internal and external surface cracks, the maximum SIF is located at the crack's center for low aspect ratios (low *a/c*) and high crack depths. For a high aspect ratio or circular springline crack, the SIF is higher near the crack's edge. The internal and external surface exhibits the opposite trend for the SIFs of crown/invert crack. If the SIF is higher than the fracture toughness, the SIF at the crack center will lead to crack depth increase, and the SIF at the crack edge will cause crack length increase.
- The aspect ratio (*a/c*) and relative crack depth (*a/t*) significantly affects the influence coefficients of surface load for internal and external surface defects.

5.2 Recommendations for Future Study

This study provides the numerical method for evaluating stress intensity factors (SIFs) of semi-elliptical internal and external surface defects of buried cast iron pipes. The SIFs were investigated for crack only and crack with corrosion defects. The semi-elliptical defects were simulated for a wide range of aspect ratios (a/c = 0.2, 0.4, 1) with relative crack depths (a/t = 0.2, 0.5, 0.8). The total depth of crack with corrosion defects was the same as crack only defects. A few recommendations for future research in this area are outlined below:

a. This study was performed for different aspect ratios and relative depths as similar to Raju and Newman (1982). Numerical studies can be performed for higher (a/c>1) and lower (a/c<0.2) aspect ratios.

b. The variation of corrosion depth for crack with corrosion defect might have an influence on SIFs. A future study can be performed by varying the corrosion depths.

c. The present study considers the springline, invert, and crown position straight cracks. The SIFs other than the mentioned position and inclined cracks can be a good option for future studies.

d. The developed model can be used for a probabilistic safety assessment of the remaining life of cast iron water mains.

References (Chapter 1, 2, and 5)

Alamilla, J. L., Espinosa-Medina, M. A., & Sosa, E. (2009). Modelling steel corrosion damage in soil environment. *Corrosion Science, 51*(11), 2628–2638. https://doi.org/10.1016/j.corsci.2009.06.052

American Water Works Association. (2017). *Buried no longer: Confronting America's water infrastructure challenge*. http://www.awwa.org/Portals/0/files/legreg/-documents/BuriedNoLonger.pdf

ASCE. (2017). *2017 Infrastructure report card: A comprehensive assessment of America's Infrastructure*. https://www.infrastructurereportcard.org/

Baird, G. M., & Folkman, S. (2019). Recent survey results of water main failures in the U.S. and Canada. In *Pipelines 2019: Multidisciplinary Topics, Utility Engineering, and Surveying, 2012*, 1–9.

Canada Infrastructure Report Card 2019. (2019). http://canadianinfrastructu-re.ca/en/about.html

Caproco Corrosion Prevention Ltd. (1985). *Underground corrosion of water pipes in Canadian cities*. Case: The city of Calgary. Report prepared for CANMET, Ottawa, Canada.

Cast Iron Soil Pipe Institute (2006). *Cast iron soil pipe and fittings handbook* (Vol. 37421, Issue 423). Cast Iron Soil Pipe Institute. www.cispi.org. Accessed on Dec. 10, 2020.

Collini, L., Nicoletto, G., & Konečná, R. (2008). Microstructure and mechanical properties of pearlitic gray cast iron. *Materials Science and Engineering A, 488*(1–2), 529–539. https://doi.org/10.1016/j.msea.2007.11.070

Conlin, R. M., and Baker, T. J. (1991). *Application of fracture mechanics to the failure behaviour of buried cast iron mains*. Contract Report No. 266, Transport and Road Research Laboratory, London.

Debnath, S. (2019). *Failure assessment of cast iron water mains using fracture mechanics* [Master`s Thesis]. Memorial University of Newfoundland.

Debnath, S., Ali, I. M., Dhar, A. S., & Thodi, P. N. (2021). Material properties for fracture mechanics based strength assessment of cast iron water mains. *Canadian Journal of Civil Engineering*, *48(1)*, 62–74. https://doi.org/10.1139/cjce-2019-0229

Debnath, S., & Dhar, A. S. (2019). Assessment of stress intensity factor for buried cast iron pipeline using finite element analysis. *72nd Canadian Geotechnical Conference (GeoSt.John's 2019), St. John's, NL, Canada. September 29 - October 2, 2019*.

Deo, R. N., Rathnayaka, S., Zhang, C., Fu, G. Y., Shannon, B., Wong, L., & Kodikara, J. K. (2019). Characterization of corrosion morphologies from deteriorated underground cast iron water pipes. *Materials and Corrosion, 70*(10), 1837–1851. https://doi.org/10.1002/maco.201910906

Fahimi, A., Evans, T. S., Farrow, J., Jesson, D. A., Mulheron, M. J., & Smith, P. A. (2016). On the residual strength of aging cast iron trunk mains: Physically-based models

for asset failure. *Materials Science and Engineering A, 663*, 204–212. https://doi.org/10.1016/j.msea.2016.03.029

Folkman, S. (2018). Water main break rates in the USA and Canada: A comprehensive study. *Mechanical and Aerospace Engineering Faculty Publications, March*, 1–49. https://digitalcommons.usu.edu/mae_facpub/174

Fu, G., Zhang, C., Deo, R., Rathnayaka, S., Shannon, B., & Kodikara, J. (2020). A model of stress concentration factors for external corrosion patches on large-diameter underground cast iron pipes. *Sustainable and Resilient Infrastructure*, *00*(00), 1–12. https://doi.org/10.1080/23789689.2020.1828022

Griffith, A. A. (1920). The phenomena of rapture and flow in soilds. In *Philosophical Transactions of the Royal Society of London* (Vol. 221, pp. 163–198). http://mbarkey.eng.ua.edu/courses/AEM644/Griffith1921fracture.pdf

Hou, Y., Lei, D., Li, S., Yang, W., & Li, C. Q. (2016). Experimental investigation on corrosion effect on mechanical properties of buried metal pipes. *International Journal of Corrosion*, *2016*. https://doi.org/10.1155/2016/5808372

Inglis, C. E. (1913). Stress in a plate due to the presence of cracks. *Meetings of the Fifty-fourth Session of the Institution of Naval Architects* (pp. 219–241).

Irwin, G. R. (1957). Analysis of stress and strain near the end of sharp corners. *Journal of Applied Mechanics*, *24*, 361–364.

Ji, J., Zhang, C., Kodikara, J., & Yang, S. Q. (2015). Prediction of stress concentration factor of corrosion pits on buried pipes by least squares support vector machine. *Engineering Failure Analysis*, *55*, 131-138.

Ji, J., Robert, D. J., Zhang, C., Zhang, D., & Kodikara, J. (2017). Probabilistic physical modelling of corroded cast iron pipes for lifetime prediction. *Structural Safety*, *64*, 62–75. https://doi.org/10.1016/j.strusafe.2016.09.004

Laham, S. A. (1998). Stress intensity factor and limit load handbook. In *British Energy Generation Ltd* (Issue 2).

Liyanage, K. T. H. (2016). *Numerical investigation of faiulre mechanisms of cast iron* [Masters Thesis]. Memorial University of Newfoundland.

Ma, Z., & Yamada, K. (1994). Durability evaluation of cast iron water supply pipes by sampling tests. *Proceeding of the Structural Engineering, Japan Society of Civil Engineers, Tokyo, 40A.*

Mahmoodian, M. (2018). Case studies on the application of structural reliability analysis methods. In *Reliability and Maintainability of In-Service Pipelines*. https://doi.org/10.1016/b978-0-12-813578-5.00005-6

Martin, J. W. (2006). Metals and alloys. In *Materials for Engineering* (pp. 71–132). https://doi.org/10.1533/9781845691608.2.71

Mondal, B. C., & Dhar, A. S. (2019). Burst pressure assessment of corroded pipelines using fracture mechanics criterion. *Engineering Failure Analysis*, *104(August 2018*), 139–153. https://doi.org/10.1016/j.engfailanal.2019.05.033

Paradkar, A. B. (2012). *An evaluation of failure modes for cast iron and ductile iron water pipes* [Masters Thesis]. The University of Texas at Arlington.

Petersen, R. B., & Melchers, R. E. (2012). Long-term corrosion of cast iron cement lined pipes. *Annual Conference of the Australasian Corrosion Association 2012*, 146–157.

Rajani, B., & Kleiner, Y. (2004). Non-destructive inspection techniques to determine structural distress indicators in water mains. *NRC Publications Archive (NPArC),* 1–20.

Rajani, B., & Kleiner, Y. (2013). External and internal corrosion of large-diameter cast iron mains. *Journal of infrastructure systems*, *19*(4), 486-495.

Rajani, B. (2000). *Investigation of grey cast iron water mains to develop a methodology for estimating service life*. American Water Works Association.

Rajeev, P., Kodikara, J., Robert, D., Zeman, P., & Rajani, B. (2014). Factors contributing to large daimeter water pipe failure. *Water Asset Management International, 10*(3), 9–14.

Raju, I. S., & Newman, J. C. (1982). Stress-intensity factors for internal and external surface cracks in cylindrical vessels. *Journal of Pressure Vessel Technology, Transactions of the ASME, 104*(4), 293–298. https://doi.org/10.1115/1.3264220

Seica, M. V., & Packer, J. A. (2004). Mechanical properties and strength of aged cast iron water pipes. *Journal of Materials in Civil Engineering*, *16*(1), 69–77. https://doi.org/10.1061/(asce)0899-1561(2004)16:1(69)

Seica, M. V., Packer, J. A., Grabinsky, M. W. F., & Adams, B. J. (2002). Evaluation of the properties of Toronto iron water mains and surrounding soil. *Canadian Journal of Civil Engineering, 29*(2), 222–237. https://doi.org/10.1139/l01-090

Siu, J. (2018). Cast iron trunk watermains in the city of Toronto. In *Pipelines 2018: Condition Assessment, Construction, and Rehabilitation* (pp. 701-707).

Usher, K. M., Kaksonen, A. H., Cole, I., & Marney, D. (2014). Critical review: Microbially influenced corrosion of buried carbon steel pipes. *International Biodeterioration and Biodegradation, 93*, 84–106. https://doi.org/10.1016/j.ibiod.2014.05.007

Vipulanandan, C., Qiao, W., & Hovsepian, H. (2011). Case studies on water pipeline failures in the active zone. *Geo-Frontiers 2011*, 1081–1090.

Wang, W., Zhou, A., Fu, G., Li, C. Q., Robert, D., & Mahmoodian, M. (2017). Evaluation of stress intensity factor for cast iron pipes with sharp corrosion pits. *Engineering Failure Analysis, 81*, 254–269. https://doi.org/10.1016/j.engfailanal.2017.06.026

Yamamoto, K., Mizoguti, S., Yoshimitsu, K., & Kawasaki, J. (1983). Relation between graphitic corrosion and strength-degradation of cast iron pipe. *Corrosion Engineering, 32*(3), 157–162. doi:10.3323/jcorr1974.32.3_157